Measurement of the Nucleon Form Factors in the Time-Like region at DAΦNE

Letter of Intent

(working version)

10 October 2005

PARTICIPATING INSTITUTIONS

ARMENIA: Yerevan Physics Institute, Yerevan

N. Apokov, R. Avakian, A. Avetisian, G. Elbakian, Z. Hakopov, H. Marukian, S. Taroian

CHINA: Shangai Institute for Nuclear Research, Shanghai

W. Xu

FRANCE: DAPNIA/SPhN, CEA/Saclay

E. Tomasi-Gustafsson

ITALY: INFN, Sezione di Bari

G. D'Erasmo, E. Fiore, A. Pantaleo, V. Paticchio

ITALY: Dipartimento di Meccanica, Università di Brescia and INFN Sezione di Pavia

G. Bonomi, A. Donzella, A. Zenoni

ITALY: INFN, Laboratori Nazionali di Frascati, Frascati

R. Baldini, L. Benussi, M. Bertani, N. Bianchi, S. Bianco, E. De Sanctis, F.L. Fabbri, A. Fantoni, P. Gianotti, V. Lucherini, M. Mirazita (*editor and contact person*), V. Muccifora, S. Pacetti, C. Petrascu, E. Polli, F. Pompili, A. R. Reolon, F. Ronchetti, P. Rossi, S. Tomassini

ITALY: INFN Sezione di Roma

G. Salmé

ITALY: Università di Roma Tor Vergata and INFN Sezione di Roma Tor Vergata

R. Messi, E. Pace

ITALY: Dipartimento di Fisica, Politecnico di Torino and INFN, Sezione di Torino

M. Agnello

ITALY: Dipartimento di Fisica Generale, Università di Torino, and INFN Sezione di Torino

L. Busso, D. Faso

ITALY: Dipartimento di Fisica Sperimentale, Università di Torino and INFN, Sezione di Torino

E. Botta, T. Bressani, S. Bufalino, F. De Mori, S. Marcello

ITALY: INAF-IFSI Sezione di Torino and INFN Sezione di Torino

O. Morra

ITALY: INFN Sezione di Torino

D. Calvo, A. Feliciello, A. Filippi

ITALY: INFN, Sezione di Trieste

M. Bregant, P. Camerini, N. Grion, G. Margagliotti, S. Piano

RUSSIA: Budker Institute, Novosibirsk

S. Eidelman, E.B. Levichev, S.I. Serednyakov, S. Skrinsky, E. Solodov

RUSSIA: Institute for Theoretical and Experimental Physics, Moscow

A. Gasparyan, A.B. Kaidalov, L. Kondratyuk

RUSSIA: Institute of Nuclear Research, Russian Academy of Science, Moscow

V. Yu. Grishina

RUSSIA: Petersburg Nuclear Physics Institute of Academy of Science

S. Belostotsky

USA: University of Virginia, Charlottesville, VA

S. Liuti

USA: Triangle University Nuclear Lab. and Duke University, Durham, NC

D. Dutta, H. Gao

USA: Thomas Jefferson National Accelerator Facility, Newport News, VA

K. de Jager, F. Gross

USA: Center for Theoretical Physics, Yale

F. Iachello

EXECUTIVE SUMMARY

The study of the electromagnetic Form Factor (FF) of the nucleon in both the space-like and time-like domains plays a key role for the understanding of the internal structure and dynamics of this basic building block of the matter. Nucleon form factors are also necessary for the interpretation of many other measurements in reactions involving nucleons. In particular, elastic form factors are a limiting case of Generalized Parton Distribution (GPD) functions and can be used to constraint GPD models.

In spite of being under investigation by more than forty years, nucleon form factors are far from being fully exploited and more efforts devoted to their experimental determination are needed. In fact, for more than 30 years it has been believed [1] that the ratio of the electric to magnetic space-like form factor of the proton G_E^p/G_M^p, as obtained with the Rosenbluth technique, was constant and approximately equal to the magnetic moment of the proton μ_p. On the contrary, recent measurements of the proton using the recoil polarization technique [2–4] have shown a dramatically different picture: the ratio G_E^p/G_M^p is monotonically decreasing with increasing Q^2 suggesting crossing the zero at $Q^2 \approx 8$ GeV. These unexpected results have produced a revival of the experimental studies and have triggered a strong theoretical interest (see [5–7] for recent reviews). The two-photon exchange contribution has been suggested to be responsible for the observed discrepancy, but the situation is still not definitely fixed.

The space-like FFs are connected by dispersion relations to the analytical structure and phases of the form factors in the time-like domain. Theories that fit space-like data make very different predictions, once extrapolated in the time-like region. Then the knowledge of the phase difference between $|G_E|$ and $|G_M|$ strongly constrain the models for both form factors.

Unfortunately, data in the time-like region are largely incomplete. $|G_M^p|$ is derived from the total cross section under the assumption $|G_E^p| = |G_M^p|$ everywhere, and the electric form factor remains completely unmeasured. Since the new space-like measurements imply that this assumption is not valid, it is necessary to carefully identify and separate the time-like $|G_E^p|$ and $|G_M^p|$ form factors by measuring the center-of-mass angular distribution of $e^+e^- \to p\bar{p}$. Despite the fundamental implications of the phases for an understanding of the connections between space-like and time-like form factors, such measurements have never been made. Moreover, available data suggest the existence of additional structures in the proton magnetic form factor, especially in the near-threshold region. For the neutron, the data are scarce. The only measurement available suggests a value of the magnetic form factor much bigger than the pQCD extrapolation from proton data.

Here, we discuss the possibility of a complete measurement of the nucleon form factors in the time-like region at Frascati with the DAΦNE e^+e^- storage ring upgraded in energy and the FINUDA detector. With minor modifications to the storage ring, it is possible to reach a 2.4 GeV center-of-mass energy and a peak luminosity of the order of 10^{32} cm^{-2} s^{-1}.

To completely determine absolute values and phases of the nucleon form factor, both $p\bar{p}$ and $n\bar{n}$ will be detected with suitable efficiency and resolution, and also the normal polarization of the outgoing baryon will be measured. The latter requires the implementation of a polarimeter in the detector. This is the most stringent experimental requirement for the detector. This implementation seems to be feasible in the FINUDA detector, which is composed by two tracking regions with a large amount of free space between them where an analyzer could be placed. The other DAΦNE detector, KLOE, has a much more compact tracking system, and the implementation of the polarimeter requires the modification of its inner part. This possibility has not been explored so far. For this reason the study has been made considering the FINUDA detector only.

With the anticipated performance of DAΦNE, it results that in about two years of data taking one will produce:

- The first accurate measurement of the proton time-like form factors $|G_E^p|$ and $|G_M^p|$;
- The first measurement of the outgoing proton polarization, to get the relative phase between $|G_E^p|$ and $|G_M^p|$;
- The first measurement of the two photon contribution from the proton angular distributions asymmetry;
- The first accurate measurement of the $e^+e^- \to n\bar{n}$ cross section;
- The first measurement of the neutron time-like form factors $|G_E^n|$ and $|G_M^n|$;
- The first measurement of the strange baryon form factors.
- An accurate measurement of the cross section of $e^+e^- \to hadrons$, that provides information on possible narrow structures close to the $N\bar{N}$ threshold.

The paper is organized as follows: first, the definitions and main properties of the nucleon FFs are shortly recalled and the present knowledge of space-like and time-like FFs is reviewed. Then, the anticipated performance of the DAΦNE ring upgraded in energy are described and the case for a complete measurement of the nucleon FFs with the FINUDA detector is discussed.

2 NUCLEON ELECTROMAGNETIC FORM FACTORS

The nucleon FFs are defined by the matrix elements of the electromagnetic current $J_\mu(x)$ of the nucleon, as in Fig. 1, according to [8]

$$\langle N(p')\,|J^\mu(0)|\,N(p)\rangle = e\bar{u}(p')\left[F_1(q^2)\gamma^\mu + \frac{i}{2M}F_2(q^2)\sigma_{\mu\nu}q^\nu\right]u(p) \qquad (1)$$

where e is the proton charge, M is the nucleon mass and $q^2 = (p-p')^2$ is the squared momentum transfer in the photon-nucleon vertex. The Dirac (F_1) and Pauli (F_2) FFs, defined in terms of elements of the Dirac equation, are normalized so that for the proton $F_1^p(0) = 1$ and $F_2^p(0) = \kappa_p = \mu_p - 1$ and for the neutron $F_1^n(0) = 0$ and $F_2^n(0) = \kappa_n = \mu_n$, where κ_p and κ_n are the anomalous part of proton and neutron magnetic moments, μ_p and μ_n respectively. Eq. (1) can be rearranged by defining the Sachs electric (G_E) and magnetic (G_M) FFs:

$$G_E = F_1 + \tau F_2 \qquad\qquad G_M = F_1 + F_2 \qquad (2)$$

where $\tau = q^2/4M^2$. In the non relativistic limit $\vec{q}^2 \to 0$, they represent the electric and magnetic distribution within the nucleon and their normalization is $G_E^p(0) = 1$, $G_M^p(0) = \mu_p$, $G_E^n(0) = 0$, $G_M^n(0) = \mu_n$.

Each Form Factor is assumed to be described by a function, which is analytic in the physical sheet of the complex q^2 plane, with a cut above the first inelastic threshold, i.e. $q^2 > (2m_\pi)^2$ for the isovector part and $q^2 > (3m_\pi)^2$ for the isoscalar part. Hence space-like FFs ($q^2 < 0$) are real, as demanded by the T-invariance, while time-like FFs ($q^2 > 0$) above the unitarity cut have a phase. The analytic structure of the time-like FF is connected by dispersion relations (DR) to the space-like regime [9–11], and also reflects the presence of hadronic resonances in the unphysical region $4m_\pi^2 < s < 4M^2$ in the $J^{PC} = 1^{--}$ channel [9], including possible gluonium, hybrid and baryonium vector states. The

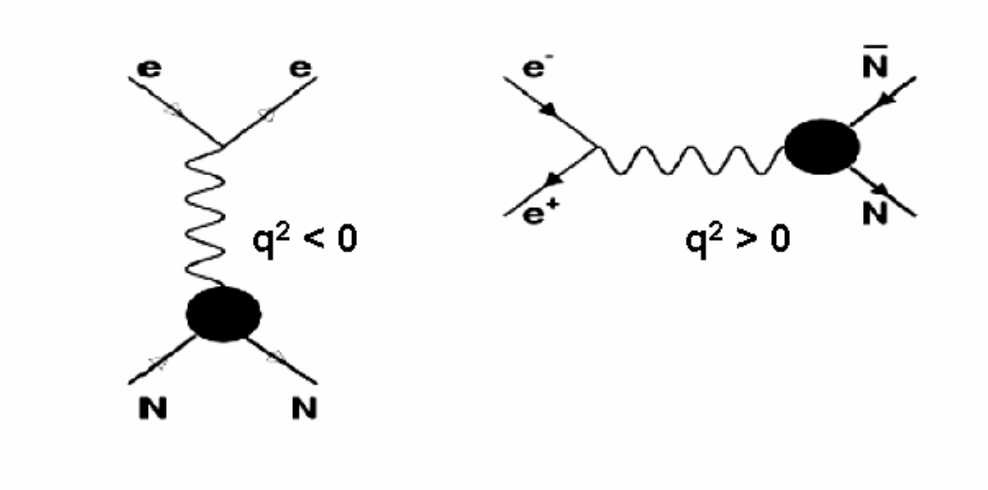

Fig. 1. *Diagrams for space-like (left) and time-like (right) electromagnetic nucleon FF measurements.*

unphysical q^2 region is large, accomodating the largest contribution, mostly due to the vector meson ground states, ρ and ω. Information on this region could be obtained without ambiguity by using dispersion relations [12], once space-like, time-like and relative phase data will be known with sufficient accuracy and over a large q^2 interval.

Furthermore, the intimate connection between the ground state observables (such as FFs) and the high energy regime (that is, between the principal quantities which so far have provided information on nuclear structure) is made explicit by the concept of Generalized Parton Distributions (GPD) [13]. These distributions, introduced nearly a decade ago, have emerged as a unique tool to describe hadrons in terms of quark and gluon degrees of freedom [14]. In fact, elastic Form Factors are a limiting case of GPDs (at small but finite Mandelstam variable t, integration over the Bjorken variable x of the H and E GPDs yields the Pauli and Dirac FFs [15]) and can be used to constraint GPD models.

The elastic lepton-nucleon scattering gives access to the space-like region, while the time-like region can be accessed in the process $e^+e^- \to N\bar{N}$ or in the reversed channel $N\bar{N} \to e^+e^-$. Radiative corrections, i.e. two-photon exchange contributions, have to be evaluated in order to get the FFs from cross section measurements, as they may give a non negligible contribution at high space-like q^2 [16–18]. In principle, two-photon contributions can be measured, for instance by comparing electron-nucleon to positron-nucleon scattering (in the space-like region) or looking for an asymmetry in the angular distribution (in the time-like region). In the space-like region, such experiment has been approved at JLab [19] and proposed at the VEPP-3 storage ring in Novosibirsk [20].

By their definition, Sachs FFs do not interfere in the expression of the cross section, therefore in the time-like case polarization observables only allow to get the relative phase (and thus to obtain the fully determination) of FFs, by using polarized beams and/or looking to initial or final state polarization observables.

2.1 **Space-like nucleon Form Factors**

Over the past several decades, a large number of experiments have measured $e^- N$ elastic scattering cross sections in order to obtain the electric and magnetic nucleon FFs using the Rosenbluth technique [21]. Basically, the FFs are extracted by linearly fitting the ϵ-dependence of the cross section at fixed Q^2

$$\frac{d\sigma}{d\Omega} = \left(\frac{d\sigma}{d\Omega}\right)_{Mott} \frac{\tau}{\epsilon(\tau-1)} \left(G_M^2 - \frac{\epsilon}{\tau} G_E^2\right), \tag{3}$$

where ϵ is the virtual photon polarization. The measurements for proton [22], shown as empty triangles in Fig. 2, indicate an approximate Form Factor scaling, i.e. $\mu_p G_E^p / G_M^p \approx 1$ up to $Q^2 \approx 7$ GeV^2, though with large uncertainties in G_E^p at the highest Q^2 values. In fact, the presence of the factor $1/\tau$ in front of G_E makes difficult its extraction when Q^2 becomes large.

Polarization measurements, employing polarized beams, polarized targets or recoil polarimeters, have been proposed several time ago as the best way to extract information on the Form Factors [23], but only in the mid of nineties, with the advent of high duty-factor polarized electron beam facilities, these experiments became possible. In particular, the elastic electron-to-proton polarization transfer measurements have been performed to obtain directly the ratio [23]

$$\mu_p \frac{G_E}{G_M} = -\mu_p \frac{P_L}{P_T} \frac{E_e + E_{e'}}{2M_p} tan(\theta_e/2), \tag{4}$$

where E_e and $E_{e'}$ are the incoming and scattered electron energies, θ_e is the electron scattering angle, P_L and P_T are the longitudinal and transverse components of the final proton polarization in the hadronic scattering plane. Because in the ratio the two polarizations are simultaneously measured, this technique avoids major systematic uncertainties of the Rosenbluth separation. It is also important to note that the contribution of the small electric FF is enhanced, because there are no suppression factors with increasing Q^2, thus allowing precision measurements also at high Q^2.

While the low Q^2 measurements at MIT-Bates [24] are consistent with the Rosenbluth data, the JLab measurements [2, 3] (shown as empty and full cir-

cles in Fig. 2), which extended the data up to $Q^2 \approx 5.6$ GeV^2, significantly deviates from the scaling behavior. In fact, they show an almost linear decrease from unity at low Q^2 up to ≈ 0.3 at the highest Q^2. The linear fit of these data, showed as a dashed curve in Fig. 2, also suggests that the electric FF should cross the zero for $Q^2 \approx 8$ GeV^2.

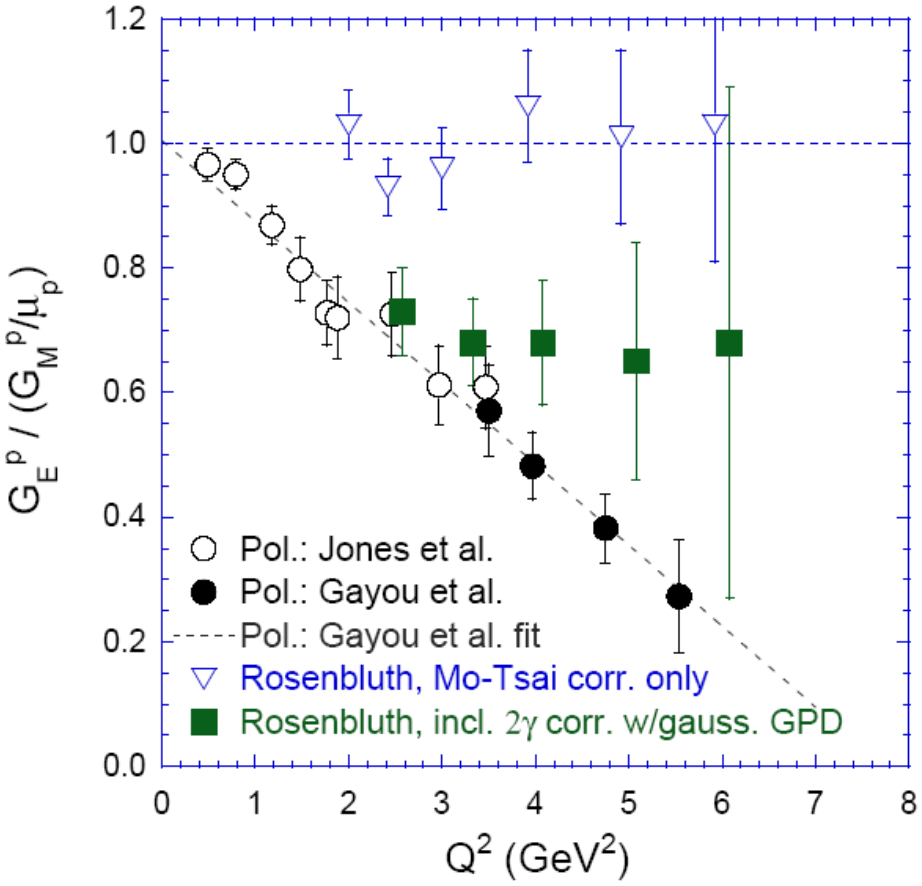

Fig. 2. *Comparison of the ratio $\mu_p G_E^p/G_M^p$ of the FFs extracted by Rosenbluth technique (hollow triangles) with recoil polarization measurements (full and empty circles) [2–4]. The dashed line is a linear fit to the polarization transfer data. Full squares are the Rosenbluth measurements corrected for two photon exchange [17]. Figure taken from Ref. [17].*

These unexpected results raise the question how to best combine data from these two techniques. A recent reanalysis of the experimental data obtained with the Rosenbluth technique [25] showed that the individual measurements are consistent to each other within small normalization uncertainty between the different experiments. The global fit of all the Rosenbluth experimental data performed in [25] confirmed the scaling of the FF as a function of Q^2, thus giving a ratio G_E/G_M well above polarization measurements. In addition, the new Rosenbluth measurement performed at JLab [26] for Q^2 between 2.6 and 4.1 GeV^2 confirmed the FF scaling, making it clear that the source of the discrepancy with polarization transfer measurements is not simply an

experimental problem.

Recent works [16–18] suggest that the possible origin of these discrepancies is the failure of the one-photon approximation to adequately describe the result of high-precision unpolarized experiments. In fact, radiative terms related to two-photon exchange corrections to the lowest order QED diagrams may result sizeable in the determination of the FFs from the differential cross section, while they should give small contribution in the polarization method. If two-photon exchange is not negligible, then the Rosenbluth formula will not represent the underlying structure of the proton, but it will be just a parametrization of the *ep* elastic cross section. An estimate done by using a quark-parton representation of the virtual photon Compton scattering [17] showed that in the range $Q^2 = 2 - 3$ GeV^2 the Rosenbluth method including two-photon exchange correction agrees well with polarization results, and at higher Q^2, there is at least partial reconciliation between the two methods (full squares in Fig. 2). Similar results have been obtained in [18]. When more detailed calculations of these corrections will be available, polarization and cross section data can be consistently combined to extract the FF without ambiguity. Other authors [27] do not find evidence of two-photon exchange contributions in the unpolarized data, in the limit of their precision, and suggest to explain this discrepancy by systematic effects due to the large radiative corrections.

New data are expected from the new polarization experiment approved at JLab [28] that will extend measurements up to $Q^2 \approx 10$ GeV^2. They will be particularly important to check the presence of a zero of G_E^p at $Q^2 \approx 8$ GeV^2, as the trend of published JLab data [2, 3] seems to suggest.

The polarization-transfer technique proved equally fruitful in applications to quasielastic scattering off polarized deuterons and ^3He as a source of information on the neutron FFs. Polarization measurements of $\mu_n G_E^n/G_M^n$ with deuteron target have been recently performed at Jlab [29]. Data are shown in Fig. 3 as full squares. As can be seen they cover only the limited range $Q^2 \leq 1.5$ GeV^2 with respect to the proton one.

Perturbative QCD (pQCD) predicts [30] for the Pauli and Dirac FFs the asymptotic behavior $F_1 \sim Q^{-4}$ and $F_2 \sim Q^{-6}$, so that $Q^2 F_2/F_1$ would reach a constant value at some high Q^2. The proton data [2, 3] clearly indicate that this regime is not reached up to $Q^2 = 5.5$ GeV^2 (neutron data doesn't cover a sufficiently high Q^2 value to draw any conclusion yet). Based on these results, the perturbative regime has been reconsidered by Miller and Frank [31], who derived the scaling law $F_2/F_1 \sim Q^{-1}$ in a relativistic constituent quark model calculation. The experimental data indicate that such a scaling law is reached at $Q^2 \sim 2$ GeV^2 [3]. On the contrary, other authors [32] found that higher twist corrections do not spoil the Q^{-6} scaling of F_2, but they just result in

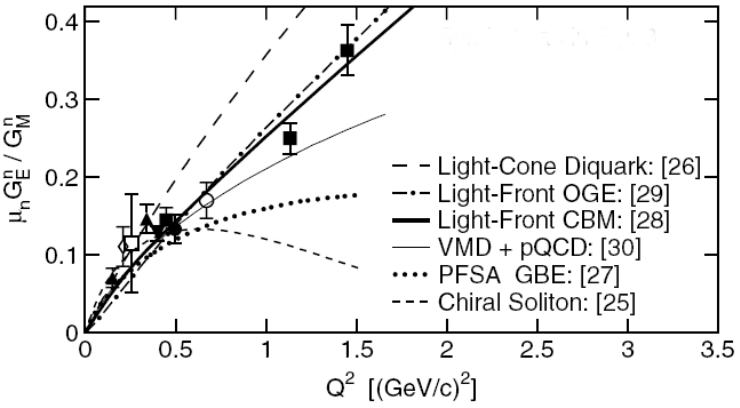

Fig. 3. *The ratio $\mu_n G_E^n/G_M^n$ as extracted by polarization measurements compared with predictions of selected models. Figure taken from Ref. [29].*

logarithmic corrections to the asymptotic pQCD scaling laws.

The theoretical models of the nucleon FFs can be grouped in two different basic approach. In the first one, the mesonic degrees of freedom are explicit, as in calculations based on vector meson dominance (VMD) [33, 34], in models comprising a three-quark core dressed with pseudo-scalar mesons [35], and in soliton model calculations [36]. Among these calculations, it is interesting to note that the model of Iachello *et al.* [34], somewhat related to the soliton models of the nucleon, predicted the observed steep decrease of the space-like G_E^p/G_M^p more than 30 years ago. The second approach consists of QCD-based quark models. These models include relativistic constituent quark (RCQM) [37], diquark [38], cloudy bag [39] and QCD sum rule [40]. All the mentioned models are based on effective theories: they all rely on a comparison with the existing (at the time of their elaboration) experimental data and their parameters are adjusted to fit the data. It is worthwhile to note that, apart from phenomenological models [41, 42], rigorous dynamical models have trouble in accurately describing all nucleon FFs, as it is necessary to fully understand the strong interaction at low energy. In fact, a successful model of confinement must be able to predict both neutron and proton FFs simultaneously. The neutron electric FF is especially sensitive to small components of the nucleon wave function, and differences between predictions for G_E^n tend to increse rapidly with Q^2, as shown by the curves in Fig. 3. New measurements on a ^3He target for Q^2 up to ≈ 4 GeV^2 are planned at JLab [43].

2.2 Time-like nucleon Form Factors

As anticipated, the time-like $G_E(s)$ and $G_M(s)$ (here and in the following, we define the total energy squared $s = q^2$), corresponding to antiparallel and parallel spin orientation in the c.m. for the outgoing baryons, are the

analytical continuation of non spin flip $G_E(Q^2)$ and spin flip $G_M(Q^2)$ space-like FFs, as defined in the Breit frame. Since time-like FFs are complex functions, while the space-like ones are real, this continuity requirement imposes strong theoretical constraints (for example time-like FFs must be asymptotically real for $s \to \infty$).

The absolute value of nucleon FFs can be derived from cross section measurements in $e^+e^- \to N\bar{N}$ experiments. In the one-photon exchange approximation, the center-of-mass total and differential cross section as a function of s are given by [44]

$$\sigma = \frac{4\alpha^2\pi\beta}{3s} C \left[\mid G_M \mid^2 + \frac{1}{2\tau} \mid G_E \mid^2 \right], \tag{5}$$

$$\frac{d\sigma}{d\Omega} = \frac{\alpha^2\beta}{4s} CD = \frac{\alpha^2\beta}{4s} C \left[\mid G_M \mid^2 (1 + cos^2\theta) + \frac{1}{\tau} \mid G_E \mid^2 sin^2\theta \right], \tag{6}$$

where θ is the proton scattering angle, $\beta = \sqrt{1 - 4M^2/s}$ is the nucleon velocity, $\tau = s/4M^2$. C is the Coulomb correction factor [45], which takes into account QED Coulomb interaction and modifies the Born approximation at threshold. It can be evaluated in the distorted wave approximation in final state interaction and is given by:

$$C = \frac{y}{1 - exp(-y)} \qquad\qquad y = \pi\alpha M/\beta\sqrt{s} \tag{7}$$

Equation (6) provides the analog of the Rosenbluth formula in the time-like region. At threshold ($s = 4M^2$) the two Sachs FFs are equal, assuming both Pauli and Dirac FFs are analytic functions with a continous behavior through the threshold, thus the cross section is isotropic at threshold. The same result is obtained assuming S-wave dominance at threshold. For $s \to 4M^2$, the factor C diverges as $1/\beta$ and makes the cross section non-zero at threshold:

$$\sigma(4M^2) = \frac{\pi^2\alpha^3}{4M^2} |G_E(4M^2)| \approx 0.1nb \tag{8}$$

This value is small, but not negligible, taken into account that, according to the present data, is $|G_E(4M^2)| \approx 0.5$. The factor C is subtle and important,

in view of the observed anomalous behaviour of the proton FF near threshold. It is worthwhile to remind that in the case of $e^+e^- \to n\bar{n}$ there is no Coulomb correction.

As in the space-like region, at high energy the cross section is dominated by the magnetic term, because of the presence of the factor $1/\tau$ in front of the electric one.

2.2.1 Proton data

Due to the low cross section involved (of the order of $\approx$ 1 nb just above threshold and rapidly decreasing with s), the requested accuracy of the experimental data did not allow a reliable independent extraction of the magnetic and electric FFs from angular distributions. Proton data have been obtained by measuring total cross section and arbitrarily assuming that the relation $|G_E^p| = |G_M^p|$, theoretically valid at threshold, holds in the whole explored energy region. Actually there are hints that the $|G_E^p|/|G_M^p|$ ratio is not constant with s. In fact, despite the large errors, experimental angular distributions [46–51] suggest large variations of $|G_E^p|/|G_M^p|$ above the threshold, thus strongly challenging the relation $|G_E^p| = |G_M^p|$. However, based on this approximation, the magnetic FF has been derived, leaving on the other hand the electric FF basically experimentally unknown.

The magnetic FF has been derived in this way by several e^+e^- [46, 48–50, 52, 53] and $p\bar{p}$ [54–58] experiments, from threshold up to 15 GeV^2; the results are shown in Fig. 4 in two different s-range. Very recently, the BaBar experiment tried the extraction of the $|G_E^p|/|G_M^p|$ by using the radiative return technique [59]. For energy square below $\approx$2.1 GeV^2, this ratio is found to be greater than unity, in disagreement with indications coming from LEAR data [55]. Nevertheless, they quoted their final result still computing the magnetic FF under the assumption $|G_E| = |G_M|$.

An unexpected feature in Fig. 4 is the steep decrease very near to the threshold. A fit to the data in this region appears to indicate the presence of a resonance with mass of 1.87 GeV/c and negligible width and gives a good description of this behavior. This possible resonance could be identified as a $N\bar{N}$ bound state, the so called baryonium, dreamed for long time, but never clearly established. By measuring both proton and neutron it may be also possible to determine the isoscalar or isovector nature of this resonance. Signals indicating steep behavior very near $N\bar{N}$ threshold have been recently found in several processes concerning scalar or pseudoscalar $N\bar{N}$ states, like J/ψ radiative decay and some B decays [59]. A vector baryonium is expected to have a small coupling to e^+e^-, if any. According to some models it is also expected to have a relatively narrow hadronic width. It can be demonstrated that such a narrow resonance,

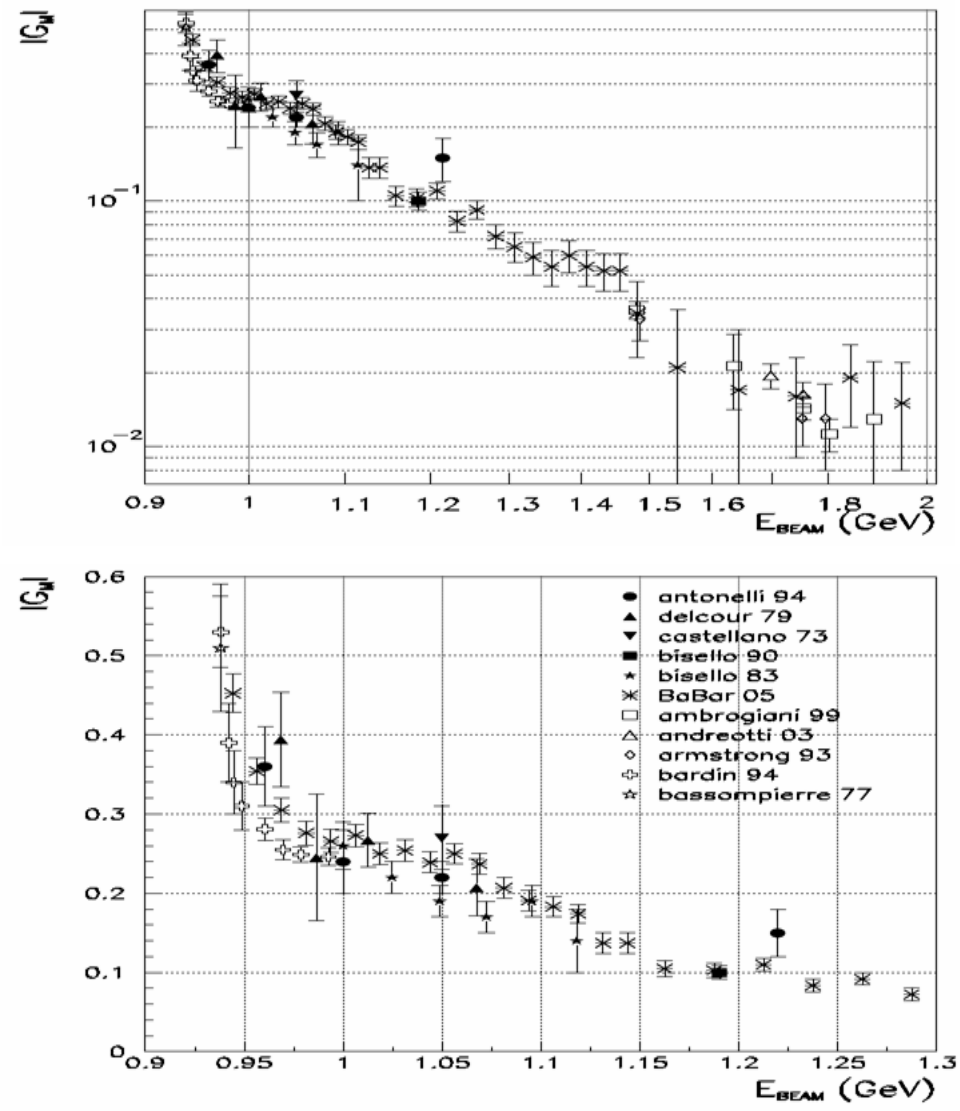

Fig. 4. *Proton magnetic FF in the timelike region with e^+e^- [46, 48–50, 52, 53, 59] (full symbols) and $p\bar{p}$ [54–58] (empty symbols) experiments under the hypothesis $|G_M| = |G_E|$ in two different energy regions.*

lying on top of a broad vector meson recurrence of ρ, ω and ϕ, should be seen as a dip in some cross section. Dips have indeed been detected in the total e^+e^- hadronic annihilation cross section and in some specific multipion channels. Dominance of pion exchange has been suggested as alternative explanation to the baryonia interpretation, giving rise to a real amplitude with a steep behavior. The origin of the steep behavior at threshold will be settled once a complete set of accurate data on both G_E^p and G_M^p, absolute value and relative phase, of the proton and neutron, will be available.

Another somewhat unexpected aspect concerns the general trend of $|G_M^p(q^2)|$: analiticity [60] and pQCD predict the time-like FF is asymptotically close to

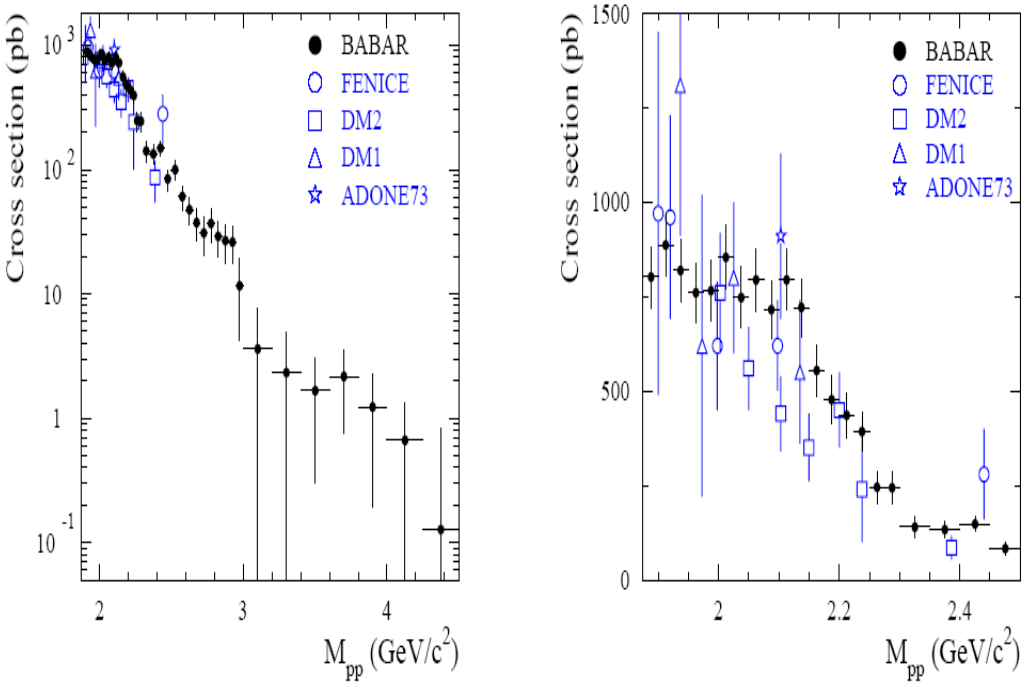

Fig. 5. *Total cross section $e^+e^- \to p\bar{p}$ as measured in two different energy regions.*

the space-like value at the same $|Q^2|$ [30]; that is, the time-like proton FF asymptotically becomes real and scales as $1/Q^4$. Experimental data are consistent with the scaling already above $Q^2 \approx$ 3-4 GeV^2, but they exceed the space-like value by a factor of 2 [61]. Some theoretical models predict qualitatively such a behaviour [62, 63]. Clearly, the uncertainty about the contribution of the electric FF might strongly affect these conclusions.
Actually the new BaBar data show a further quite unexpected cross section reaching the asymptotic trend by means of negative steps, at $\sqrt{s} \approx 2.2$ GeV and at $\sqrt{s} \approx 2.9$ GeV, as shown in Fig. 5 [59].

2.2.2 Neutron data

The neutron magnetic FF has been measured by the FENICE experiment [47] only from threshold up to $s = 4.4$ GeV^2 with low statistics (about 100 $n\bar{n}$ events collected). The results are shown in Fig. 6.
For the neutron magnetic FF, pQCD predicts the limit $|G_M^p| \approx (q_u/q_d)^2|G_M^n| = 4|G_M^n|$, that is a cross section $\sigma(e^+e^- \to p\bar{p})$ almost four times bigger than $\sigma(e^+e^- \to n\bar{n})$. On the contrary, despite the large statistical errors, the FENICE data clearly show that above threshold the $n\bar{n}$-production cross section is almost twice as $p\bar{p}$ one, indicating that the neutron magnetic FF should be much bigger than the pQCD extrapolation from proton data (shown in Fig. 6 as full line). Within the scant FENICE statistics, the neutron electric FF is consistent with zero at threshold. In such a case the neutron magnetic FF should also be zero, and this is consistent with the present data.

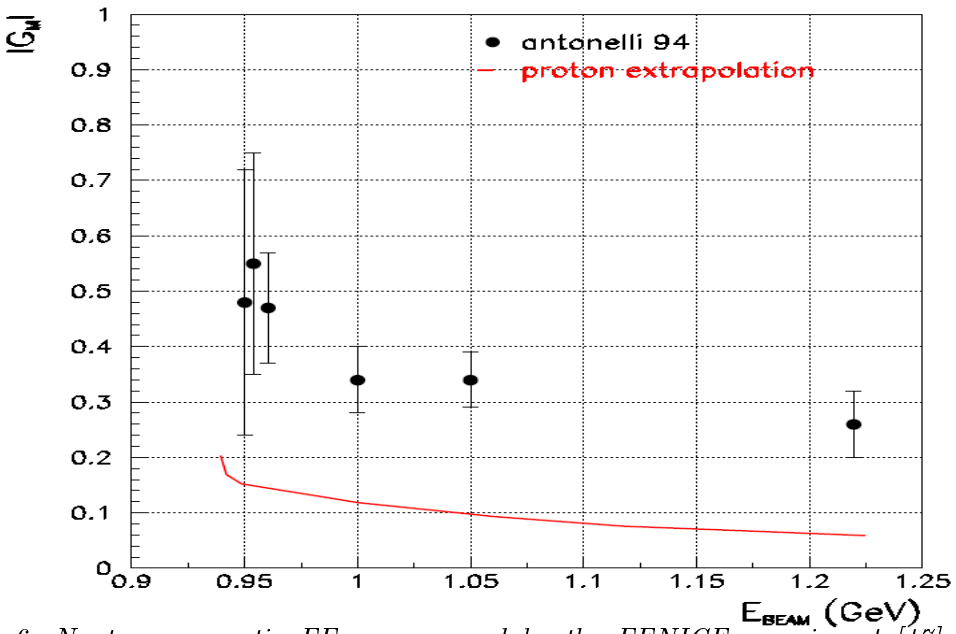

Fig. 6. *Neutron magnetic FF as measured by the FENICE experiment [47] (red circles), compared with the pQCD extrapolation from proton data (red line).*

2.2.3 Complex phases

The relative phase between G_E and G_M (and therefore between F_1 and F_2) can be accessed only via single- or double-polarization experiments [44, 64, 65]. The complex nature of time-like FFs makes it possible for the outgoing nucleon to be polarized normally to the scattering plane even without any polarization in the initial state. This polarization is given by [44, 65]

$$P_y = \frac{sin2\theta}{D\tau}\ \Im\left(G_E^* G_M\right) = \frac{sin2\theta}{D\tau}\ \mid G_E \mid \mid G_M \mid sin\delta_{ME}, \tag{9}$$

where D is defined in eq. (6). It is directly related to the phase difference δ_{ME} between the two FFs and, due to the presence of the factor $sin(2\theta)$, it takes its maximum value close to the scattering angles of 45^o and 135^o, and vanishes at 90^o. Once this phase is known, by measuring the ratio of the two components of the nucleon polarizations in the scattering plane with longitudinally polarized beams, the ratio $|G_E|/|G_M|$ can be directly obtained with small systematic uncertainties, in analogy with the space-like region. Polarization measurements have never been performed so far, mainly because of the low cross section involved.

2.2.4 Theories and Models

Proton and neutron time-like FFs, despite the large uncertainties of data, seem to be in general disagreement with pQCD predictions, in particular for the proton to neutron ratio. On the contrary, phenomenological models may give predictions in agreement with the data. As an example, models inspired to the Extended Vector Dominance Model [62] predict the ratio between neutron and proton FFs in the range 1-10, depending on the location of the vector meson recurrences that are not well established. Models inspired to the Skyrme model [63] predict that this ratio should be close to 1.

Recently, phenomenological models [34, 65, 66], originally developed in the space-like region and all consistent with the polarization measurements of the $G_E^p(q^2)/G_M^p(q^2)$ ratio, have been extended to predict FFs in the time-like region. While their predictions agree for $q^2 < 0$, they disagree in the $q^2 > 0$ region, as shown by Fig. 7. In all these models, the decrease of the ratio of FF for $q^2 < 0$ is related to a cancellation between Pauli and Dirac FFs, which corresponds to an enhancement for $q^2 > 0$. Each of the models predicts a specific fall-off and phase structure of the FF and gives rise to a significant $sin^2(\theta)$ dependence in the differential cross section. Thus a non negligible nucleon polarization is expected and with a distinct s-dependence, which strongly discriminates between the different analytic forms used to fit the G_E^p/G_M^p data in the space-like region. This is clearly illustrated in the top panel of Fig. 8, where predictions [65] for the normal polarization P_y at $\theta = 45^o$ for different FF extrapolations are shown. Hence measurements of polarization observables in the time-like region may strongly discriminate among theories and models that give similar predictions in the space-like region.

Information on the FF in the time-like region are provided also by dispersion relations, which connect the real and the immaginary parts of the scattering amplitude through integral equations. Starting from the space-like polarization data of the ratio G_E^p/G_M^p and from the theoretical constraints on the FFs, the ratio between electric and magnetic FF and their relative phase have been obtained in the whole q^2 plane [12]. In Fig. 7 and 8, the results of this calculation are reported as bands. The interesting feature of this result is that the calculation gives $|G_E^p|$ a few times bigger than $|G_M^p|$ just above threshold, thus suggesting that the FF extractions performed so far assuming $|G_E^p| = |G_M^p|$ should be wrong.

2.2.5 Summary on time-like data

In summary, time-like FFs are poorly known experimentally, the neutron data are very scarce and polarization data, directly connected with the complex phases of FF, are not available at all. Proton FFs themself, even having been

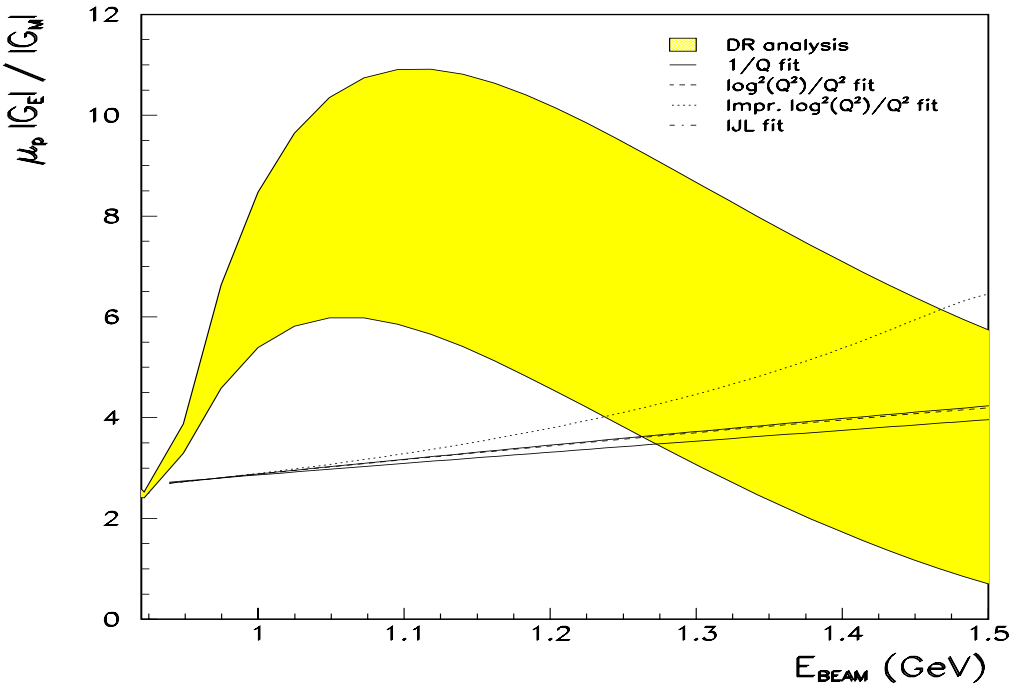

Fig. 7. *Theoretical predictions for the ratio of electric to magnetic proton FF in the time-like region as a function of the beam energy. The shadow area is the result of the dispersion relation analysis [12]. See ref. [65] for details on the other curves based on QCD models.*

the most extensively studied, rely on approximations that are not justified. This is clearly shown in Fig. 9, where, given the $e^+e^- \to p\bar{p}$ cross section from a qualitative fit of the experimental data, the FF extraction for two different hypotheses on the ratio between electric and magnetic FFs has been done. The black curve corresponds to $|G_M^p|$ assuming $|G_E^p| = |G_M^p|$, the blue and the red shaded areas are the result obtained respectively for $|G_E^p|$ and $|G_M^p|$ by using the ratio of the FF taken from the dispersion analysis [12]. As can be seen, a magnetic FF up to a factor of ≈ 2 lower can be obtained.

As said above, the contribution of the two-photon exchange diagrams has been invoked in the space-like region to partially reconcile the discrepancy between data from Rosenbluth and polarization techniques [16–18]. In the time-like region, it leads to an asymmetry in the angular distribution (relative to the incident electron direction) of the nucleon with respect to the antinucleon. An effect of the order of few percent could be estimated, also taking into account that $\gamma\gamma \to p\bar{p}$ cross section is of the same order of magnitude as for $e^+e^- \to p\bar{p}$ [67].

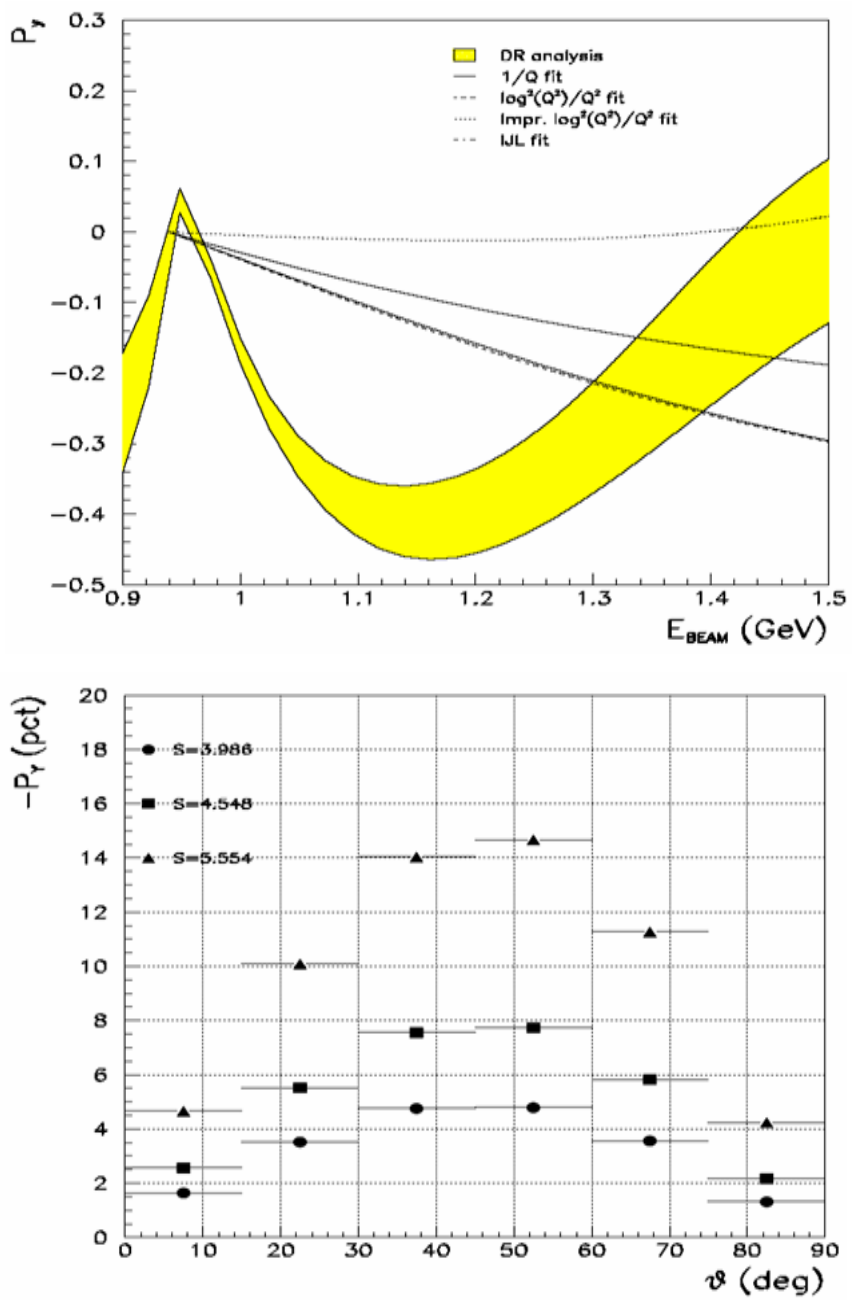

Fig. 8. *Top panel: theoretical predictions for proton polarization* P_y *at* $\theta = 45^o$ *as a function of the beam energy. Bottom panel: average polarization* P_y *as a function of the proton polar angle according to eq. 9 and normalized to the improved* $log^2(Q^2)/Q^2$ *fit.*

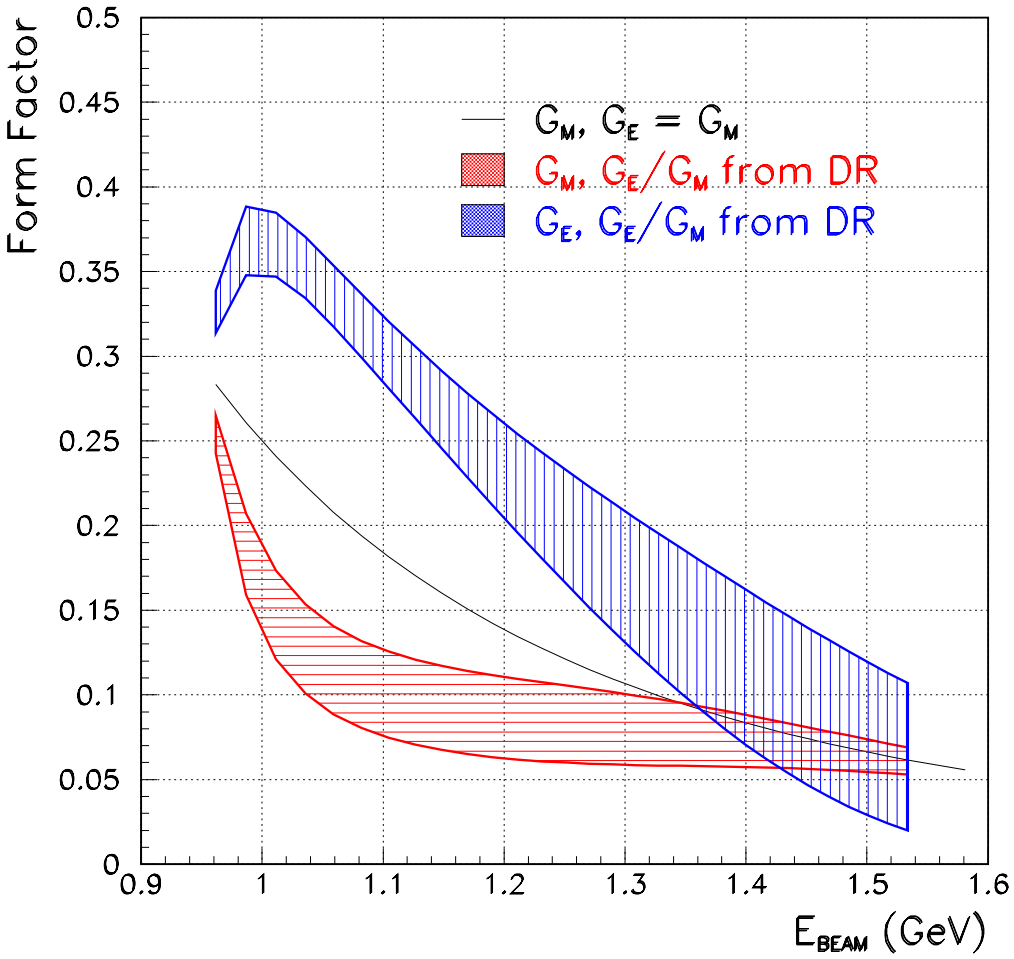

Fig. 9. *Proton FF extraction from cross section using different assumptions on the ratio between electric and magnetic FF: using* $|G_E^p| = |G_M^p|$ *(black curve), or their ratio as computed from dispersion relation analysis of [12] (red and blue areas for* $|G_M^p|$ *and* $|G_E^p|$*, respectively).*

3.1 The energy upgrade of the DAΦNE collider

The feasibility of the energy upgrade of the DAΦNE collider is discussed in [68], with maximum beam energy of 1.2 GeV per beam and peak luminosity of 10^{32} s^{-1} cm^{-2}. The main changes in the machine concern the dipole magnets and the interaction region. Some of the DAΦNE parameters are reported in Fig. 10, for all the details we refer to [68].

Maximum energy	E_{max}	GeV	1.2
Luminosity at E_{max}	L	cm^{-2} sec^{-1}	10^{32}
Injection energy	E_{inj}	GeV	0.51
Current	I	A	0.5
Number of bunches	N_b		30
Particles per bunch	N		$3.1\ 10^{10}$
Horizontal emittance	ε	mm mrad	0.6
Horizontal beta at IP	β_x^*	m	1
Vertical beta at IP	β_y^*	cm	2
Coupling	κ		0.007
Natural energy spread at E_{max}	σ_E/E		$6.6\ 10^{-4}$
Momentum compaction	α_c		0.014
Natural bunch length at E_{max}	σ_L	cm	1.9
Rf frequency	f_{rf}	MHz	368
Peak rf voltage	V	MV	0.30
Max RF power per beam	P	KW	75

Fig. 10. *Main DAΦNE parameters for 1.2 GeV operation.*

3.2 Detector requirements

Fig. 11 shows the qualitative behaviour of the total cross section data for $e^+e^- \to h\bar{h}$ above the nucleon-antinucleon threshold for the production of nucleon and hyperon pairs. The three vertical arrows indicate the thresholds for $N\bar{N}$ ($s \approx 3.5$ GeV^2), $\Lambda\bar{\Lambda}$ ($s \approx 5$ GeV^2) and $\Sigma\bar{\Sigma}$ ($s \approx 5.7$ GeV^2) production.

As can be seen, the exclusive total cross sections involved in the energy region of interest are of the order of $\approx 0.1 - 1$ nb, thus high intensity beams, with luminosity of the order of $10^{32}\ cm^{-2}s^{-1}$, are necessary in order to get accurate measurements of the angular distributions.

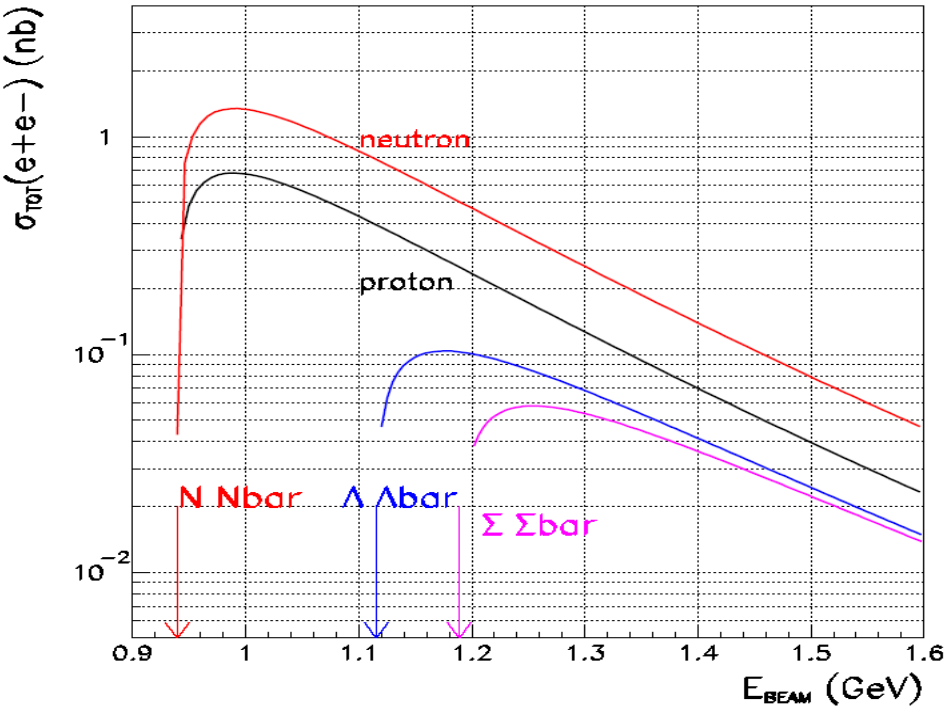

Fig. 11. *Total cross section for* $e^+e^- \to h\bar{h}$ *above nucleon-antinucleon threshold. For proton, neutron and* Λ*, the curves are normalized to the experimental data, the curve for* Σ *is extrapolated from the one for* Λ*.*

Beam polarization is not mandatory, nevertheless, if available, it will help in the extraction of the FF with smaller systematic uncertainty. For example, with longitudinally polarized beams, measuring the longitudinal (P_z) and sideways (P_x) components of the nucleon polarization, one could directly derive the ratio $|G_E|/|G_M|$ [44], as done at JLab in the space-like region (provided the relative electric to magnetic FF phase is known). On the other hand, a measurement of the normal polarization P_y with transversely polarized beams would give access to combinations of absolute value and phase of the FF different from that of eq. (9).

The clear identification of the exclusive final state requires a large acceptance detector with suitable resolution for both charged and neutral particles. Given the low cross sections involved, the detector should allow the identification of

exclusive $p\bar{p}$ and $n\bar{n}$ final states by detecting only one of the two final hadron, thus assuring a high total detection efficiency. For the $p\bar{p}$ final state, one could measure the track (i.e. the momentum) of one of the two protons, while in the case of $n\bar{n}$ the choice of detecting the neutron or the antineutron annihilation star is not obvious. In the latter case, a suitable antineutron converter (that could help for the $p\bar{p}$ detection too) should be added; it should have a high cross section for $n\bar{n}$-annihilation, a low charged pion absorption, a high conversion efficiency for neutral pions, and be amagnetic.

The detector must allow at the same time the measurement of polarization observables, in order to get information on the relative phase between electric anf magnetic FFs. Given the design of the detectors presently installed on the DAΦNE ring, KLOE [69] and FINUDA [70], this seems to be the most stringent experimental requirement. Basically, a polarimeter is composed by two tracking devices, one of which is placed after a scatterer (usually, for charged particles, a thin layer of carbon), and one needs to measure the scattering angle with respect to the scatterer plane. The implementation of such a detector seems to be feasible within the present FINUDA geometry, since this detector is already composed by two tracking regions, as shown in Fig. 12, with a large amount of free space between them where the carbon analyzer could be placed. On the contrary, being a much more compact detector (Fig. 13), KLOE does not allow an easy implementation of such a kind of polarimeter within its tracking system. The only possibility seems to be the modification of the detector close to the interaction region, with the installation of a completely new vertex tracking system followed by the carbon analyzer. This possibility has not been explored so far. For this reason, in the following Sections it will be shown how the nucleon FFs can be measured at DAΦNE-2 by using the FINUDA detector.

3.3 **The FINUDA detector**

The FINUDA detector at DAΦNE (Fig. 12) has been constructed for studying Λ-hypernuclei levels and lifetimes. Λ-hypernuclei are produced by stopping negative K^- from Φ-decays in a thin target, with the prompt π^- whose momentum is uniquely related to the energy level of the hypernucleus. The detector is conceived so as to minimize the amount of material crossed by particles to reduce as much as possible the energy straggling and multiple scattering. It is a magnetic non-focusing spectrometer with cylindric symmetry around the beam line. It can be divided in the vertex, tracking and outer regions.

The vertex region is composed by:

- the TOFino: a little barrel of 12 scintillators, 0.2 cm thick and 12 cm long,

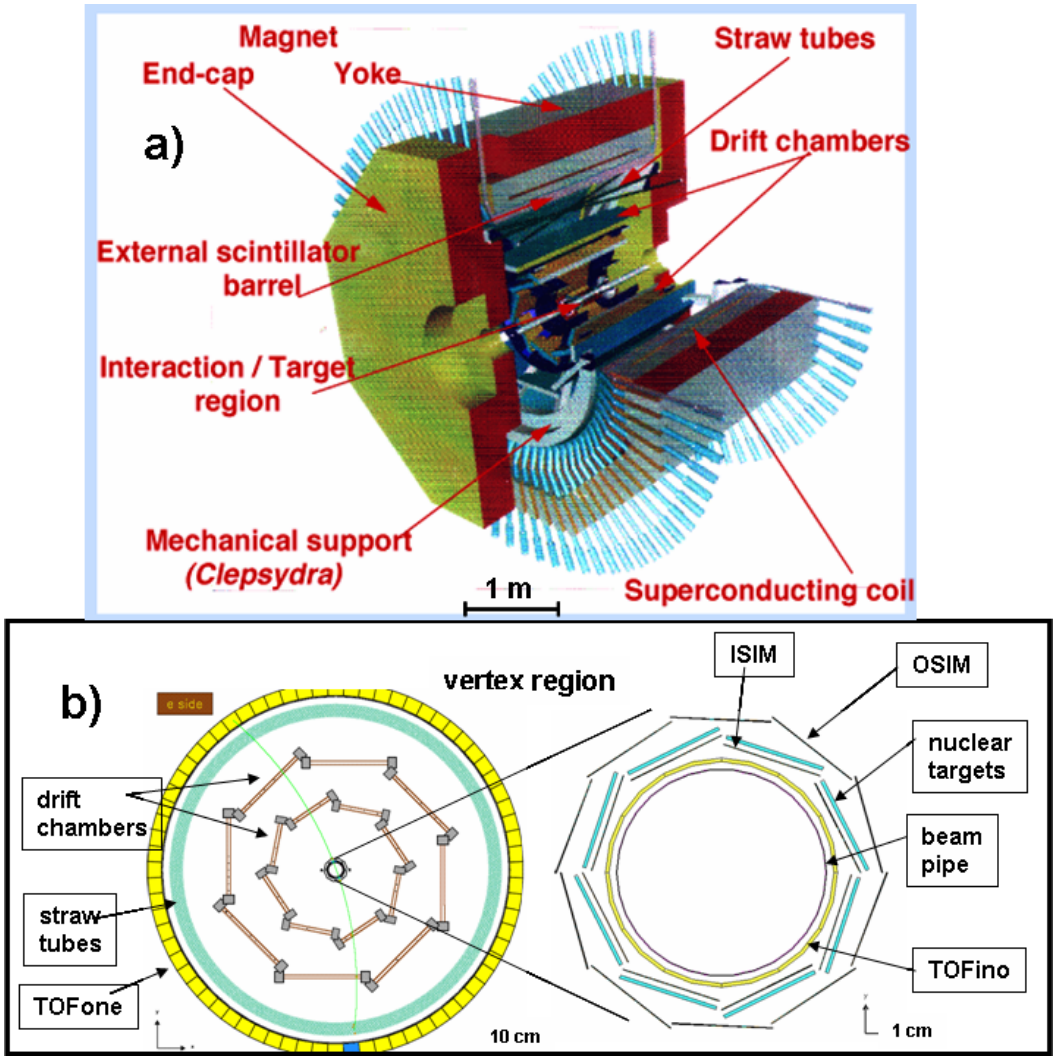

Fig. 12. *a) Layout of the FINUDA detector. b) Front view of the detector (left) and expanded view of the inner region (right).*

at 5.8 cm from the beam;

- the inner silicon microsptrip module (ISIM): 8 modules of Si microstrips, 300 μm thick, at 6.3 cm from the beam;
- the stopping target: 8 tiles of solid materoals, facing the ISIM modules.

The tracking region is composed by:

- the outer silicon microstrip detector (OSIM): 8 modules of Si microstrips, 300μm thick, at 8.3 cm from the beam;
- the low-mass drift chambers: two series of 8 drift chambers, 6 cm thick each, 43 and 75 cm from the beam;

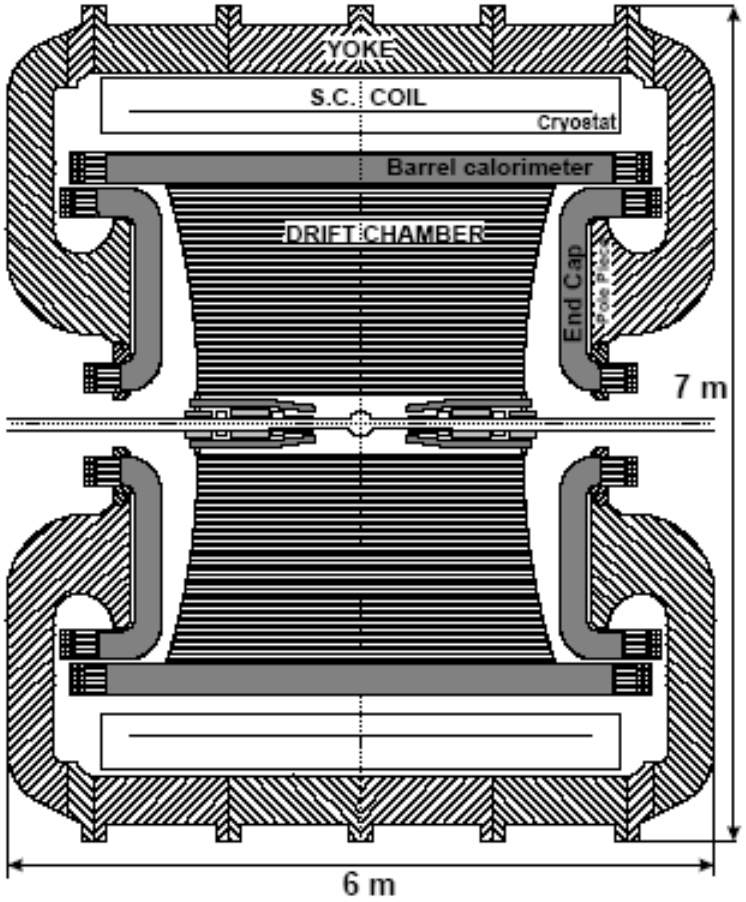

Fig. 13. *Layout of the KLOE detector.*

- an array of straw tubes: 6 layers following three orientations, for a total thickness of 16 cm, at 111 cm from the beam.

The outer region is composed by:

- the TOFone: 72 scintillator slabs, 10 cm thick, arranged as staves of a cylindric barrel at 127 cm from the beam. This detector has an efficiency for the neutron detection of about 15%;
- the magnetic coil: iron, at 138 cm from the beam, which can provide a magnetic field up to 10 kgauss.

The whole detector is immersed in Helium atmosphere, to minimize the multiple scattering. For the detection of $e^+e^- \to N\bar{N}$ this atmosphere is not needed and the targets for hypernuclear experiments must be removed. Moreover, a suitable carbon analyzer/converter must be placed within the tracking region; the easiest resort could be to insert a carbon cylinder just beyond the OSIM detector.

In the following chapters, we will make preliminary estimates of the expected

counting rates using reasonably assumptions on the $e^+e^- \to h\bar{h}$ cross sections and on the beam luminosity. For a sake of comparison, we remind that in the last twelve months the KLOE experiment has collected, at the Φ mass, an integrated luminosity of about 1800 pb^{-1}, with average luminosity of few $\sim 10^{31}$ cm^{-2} s^{-1}.

4 THE ABSOLUTE VALUE OF FORM FACTORS: CROSS SECTION MEASUREMENT WITH THE FINUDA DETECTOR

4.1 $e^+e^- \to p\bar{p}$ reaction

Taking into account the amount of material crossed by the outgoing protons, the FINUDA vertex region materials will stop protons with kinetic energy up to ≈ 17 MeV/c^2, and considering a 1.5 cm thick carbon converter, needed for the polarimeter and/or antineutron converter, the proton detection threshold can be estimated at ≈ 40 MeV/c^2, corresponding to a beam energy of 980 MeV. Then, in order to measure the FFs very close to the threshold, dedicated proton runs with beam energy below 1 GeV can be done removing the carbon converter.

A small magnetic field (of the order of few kgauss) is necessary to measure the momentum of at least one of the two final nucleons. A preliminary Monte Carlo calculation shows that the FINUDA momentum resolution (σ_p) for proton in the range of our interest is below 40 MeV/c, sufficient to distinguish exclusive $p\bar{p}$ events from the $p\bar{p}X$ background.

To estimate the expected counting rate and the attainable precision in the FF extraction, we used eq. (6) normalized to the total cross section value given by the qualitative fit of Fig. 11. We used two assumptions for the electric- to magnetic-FF ratio, $|G_E^p| = |G_M^p|$ or the value given by the dispersion relation analysis of Fig. 7 [12]. From this *theoretical* distribution, we extracted randomly the number of events as a function of the proton angle, obtaining angular distributions like those shown, as an example, in Fig. 14 for three different beam energies and for an integrated luminosity of 100 pb^{-1}. Here, we assumed a constant detection efficiency close to 1 for all polar angles, and a geometrical azimuthal acceptance $\epsilon_p \approx 0.85$ (mainly due to the drift chamber supports). Given the angular dependence of the cross section, the maximal $|G_E^p|$ contribution is at $\theta \approx 90^o$; thus the FINUDA angular coverage does not represent a relevant limitation for $|G_E^p|$ measurement.

The angular distributions have been fitted over the FINUDA angular coverage

$\theta = 45^o - 135^o$ with the function

$$f(\theta) = A(1 + cos^2\theta) + Bsin^2\theta, \tag{10}$$

and $|G_M^p|$ and $|G_E^p|$ have been directly extracted from the coefficients A and B, respectively. These fits are shown by the full curves in Fig. 14. In order to properly take into account the correlation between the two coefficients of eq. (10), we repeated this procedure for several samples of the same distribution. The mean value and the width of these distributions give an estimate of the average value and the error on the FF extraction. The relative error resulting from this procedure is shown as a function of the integrated luminosity for $E_{BEAM} \approx 1.2$ GeV in Fig. 15 for both $|G_M^p|$ (circles) and $|G_E^p|$ (squares). A few percent error on the FFs can be achieved from threshold up to $E_{BEAM} \approx 1.2$ GeV with an integrated luminosity of 100 pb^{-1}, which corresponds, with the actual performance of the DAΦNE accelerator, to less than 20 days of data taking.

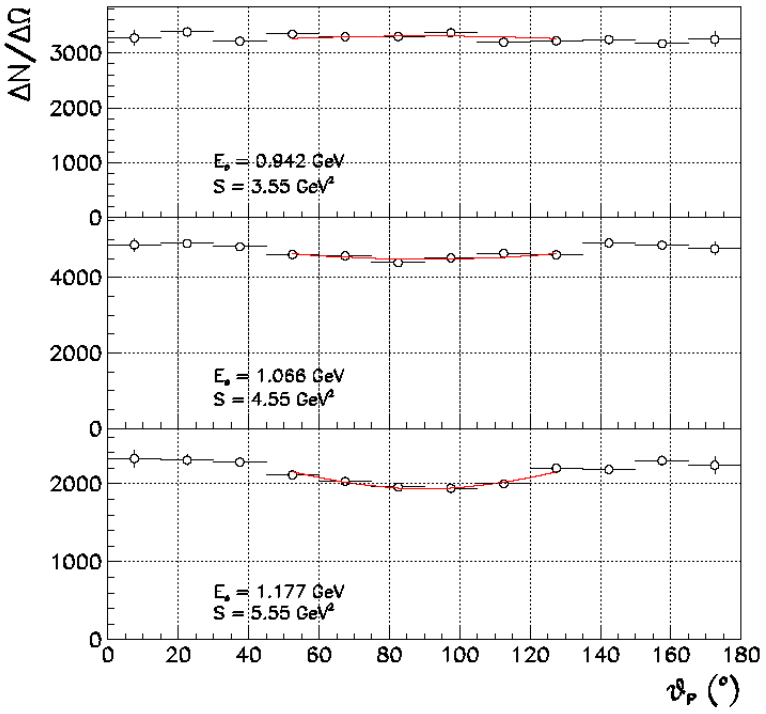

Fig. 14. *Projected angular distributions for $e^+e^- \to p\bar{p}$ at three different beam energies, assuming the electric and magnetic FFs are equal, detection efficiency ϵ_p = 0.85 and integrated luminosity of* $100pb^{-1}$ *. The full line is a fit of the data with eq. (10) in the FINUDA angular range.*

Supposing to make an energy scan of five values from threshold up to ≈ 1.2 GeV, in about five months one can measure both electric and magnetic FFs

of the proton at a few percent level.
The projected values of the magnetic FF are shown in Fig. 16, compared with presently available data. We also note that a measurement with an accuracy at the level of few percent should evidentiate possible asymmetries in the proton angular distributions with respect to the antiproton ones due to the two-photon contributions in the cross section.

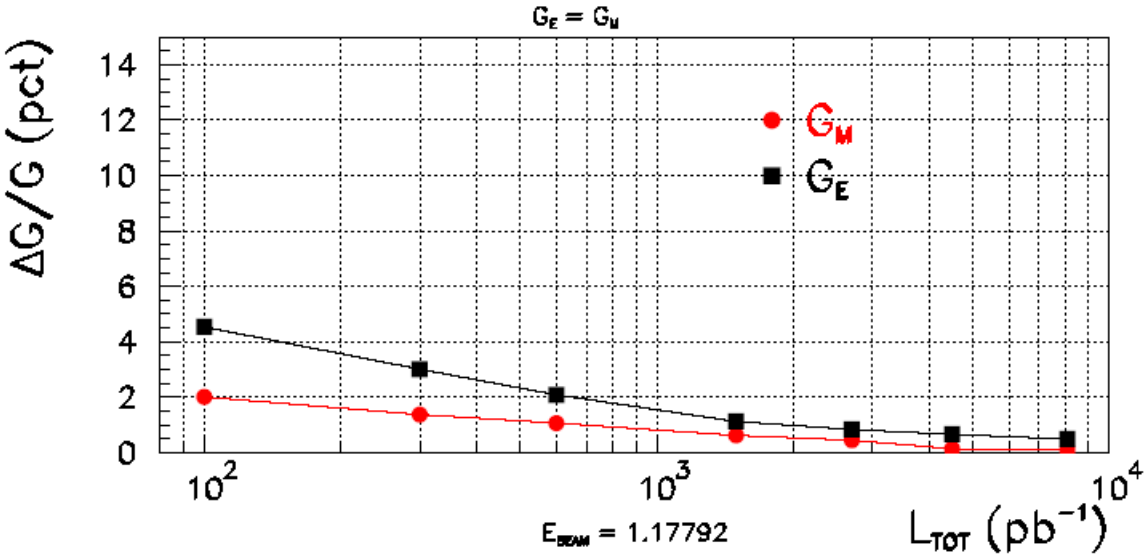

Fig. 15. *Relative error on the proton FFs as a function of the integrated luminosity for* E_{BEAM}*=1.2 GeV.*

4.2 $e^+e^- \to n\bar{n}$ **reaction**

As mentioned above, the identification of the $n\bar{n}$ final state can be performed either detecting the neutron or the $\bar{n}$ annihilation star. With the FINUDA detector, neutrons can be detected by the scintillators of the TOFone system, with an average detection efficiency of the order of 15%, weakly depending on the neutron energy. Willing to detect the $\bar{n}$ star, a carbon converter can be used to increase the annihilation probability. The choice of 1.5 cm of carbon seems optimal, because the same material can be used for the proton polarimeter as well. Preliminary simulations [71] show that antineutrons with kinetic energy below $\approx$ 30 MeV primarily annihilate in the vertex region of the FINUDA detector. Thus, it seems convenient to place the carbon converter immediately beyond the OSIM array, around 9 cm from the beam. In this way the annihilation charged products emitted towards the outer part of the apparatus can be also traced. The estimated neutron detection efficiencies are given in Tab. 1 [71]; they range from around 30% at threshold down to

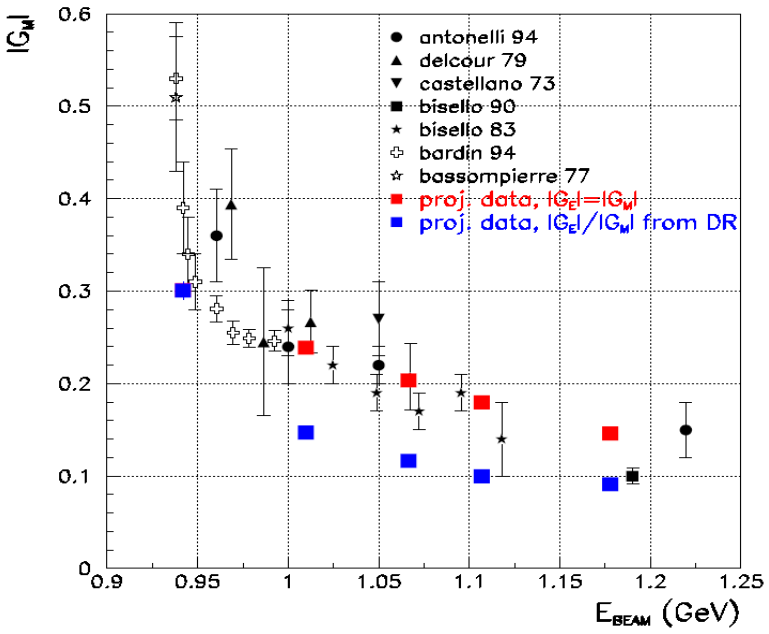

Fig. 16. *Projected proton magnetic FF results for the two hypothesis on the electric to magnetic FFs ratio, compared with actual experimental values.*

$\sqrt{s}$ [MeV]	ϵ_n [%]	ϵ_n^{COINC}[%]
1879.13	31	4.7
1880	24	3.6
1890	16	2.4
1900	13	2.0
1920	8	1.2
1940	6	0.9
2000	6	0.9
2400	6	0.9

Table 1
Detection efficiency for $e^+e^- \to n\bar{n}$ by identifying the annihilation antineutron star only (second column) or with neutron detection coincidence (third column) as a function of the total energy.

6% for neutron kinetic energy of 40 MeV and higher. These numbers indicate that close to the threshold the detection of the $\bar{n}$ annihilation should give the higher efficiency, while as the energy increases probably it will be preferably to detect the neutron. The detection of both nucleons in coincidence, though helping in reducing the background, will strongly decrease the efficiency at a level of $\approx 1\%$.

To estimate the counting rate and the error on the FF extraction, we followed the same procedure adopted for the proton. We started from the qualitative fit of the cross section in Fig. 11 and the differential cross section of eq. (6). In this case, we made two assumption on the FF, the first one is $|G_E^n| = 0$, as the FENICE data [47] suggest, the second one is $|G_E^n| = |G_M^n|$, in analogy with what has been done for the proton. We also assumed a constant detection efficiency $\epsilon_n = 0.15$. An example of the resulting angular distributions for three beam energies are shown in Fig. 17 for a total integrated luminosity of 100 pb^{-1}. These distributions have been fitted to eq. (10) for angles between 45^o and 135^o (the FINUDA coverage), and then the FFs have been extracted from the two parameters A and B.

By repeating this procedure for several samples of the same angular distributions, we estimated the error on the FF extraction shown in Fig. 18 for $E_{BEAM} \approx 1.2$ GeV. As can be seen, the neutron FFs can be extracted with errors below 10% with an integrated luminosity of the order of 100 pb^{-1}. The projected attainable $|G_M|$ values are shown in Fig. 19, compared with the FENICE experimental data.

5 THE PHASE OF PROTON FORM FACTORS: POLARIZATION MEASUREMENT WITH THE FINUDA DETECTOR

The proton polarization can be measured through secondary scattering of the emitted proton in a strong interaction process, where the spin-orbit coupling causes an azimuthal asymmetry in the scattering. The scattering cross section is given by

$$\frac{d\sigma}{d\Omega} = \sigma_0(\theta_s, T)[1 + A(\theta_s, T)\ (P_{y'}^C\ cos\phi_s + P_{x'}^C sin\phi_s)], \tag{11}$$

where θ_s and ϕ_s are the angles of the scattered proton with respect to the initial direction and $\vec{P^C}$ is the polarization vector on the polarimeter plane (defined by the axis x' and y', while z' is parallel to the emitted proton direction). The passage of protons through the analyzer is largely dominated by small angle multiple scattering, thus an angular cut at small angles has to be set, leading to polarimeter efficiency of the order of few percent [72]. The function $A(\theta_s, T)$ in eq. (11) is the analysing power of the material. A commonly used material for polarimeter is carbon, for which the analysing power is well known at least up to 20^o for proton kinetic energy from few tenth of MeV up to 1 GeV [72].

Referring to the FINUDA geometry (sketched in Fig. 20), the carbon analyzer should be placed just beyond the OSIM detector. The first tracking system is composed by the FINUDA vertex region and the OSIM detector and the second one by the two layers of drift chambers and the straw tubes. Since the

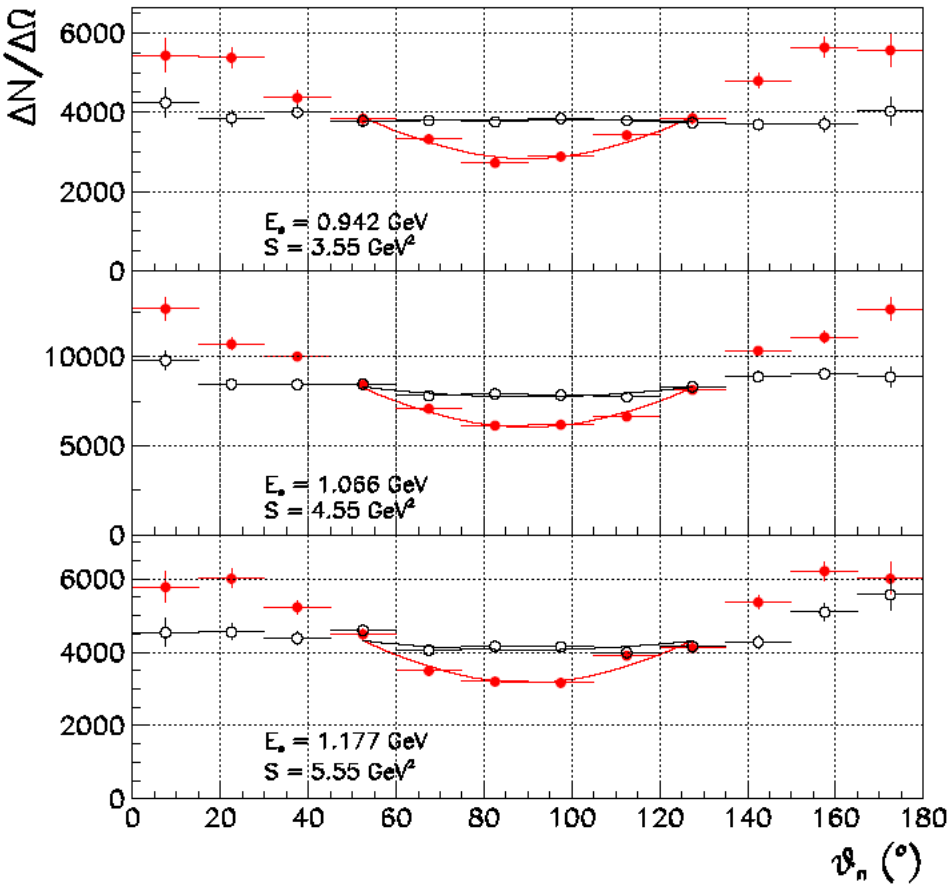

Fig. 17. *Projected angular distribution for* $e^+e^- \to n\bar{n}$ *at three different beam energies, assuming the electric and magnetic FFs are equal (full circles) or* $|G_E^n| = 0$ *(open circles), a detection efficiency* $\epsilon_p = 0.15$ *and an integrated luminosity of* $100pb^{-1}$ *. The full line is a fit of the data to eq. (10) over the FINUDA angular coverage.*

proton and the antiproton are back-to-back, one could use also the antiproton hits to reconstruct the initial proton track.

The FINUDA detector is immersed in a magnetic field (momentum measurement is necessary to select exclusive events), then the proton polarization at the interaction point $\vec{P}$ undergoes a precession around the direction of the magnetic field. The result is that the measured polarizations $P_{x'}^C$ and $P_{y'}^C$ in eq. (11) will be functions of the initial polarization $\vec{P}$, that, knowing the field map, can be exactly computed. With unpolarized electron beams, the proton polarization vector has the normal component P_y only, then $P_{x'}^C$ and $P_{y'}^C$ will be directly proportional to P_y.

Experimentally, the polarization P_y on the polarimeter plane is obtained by

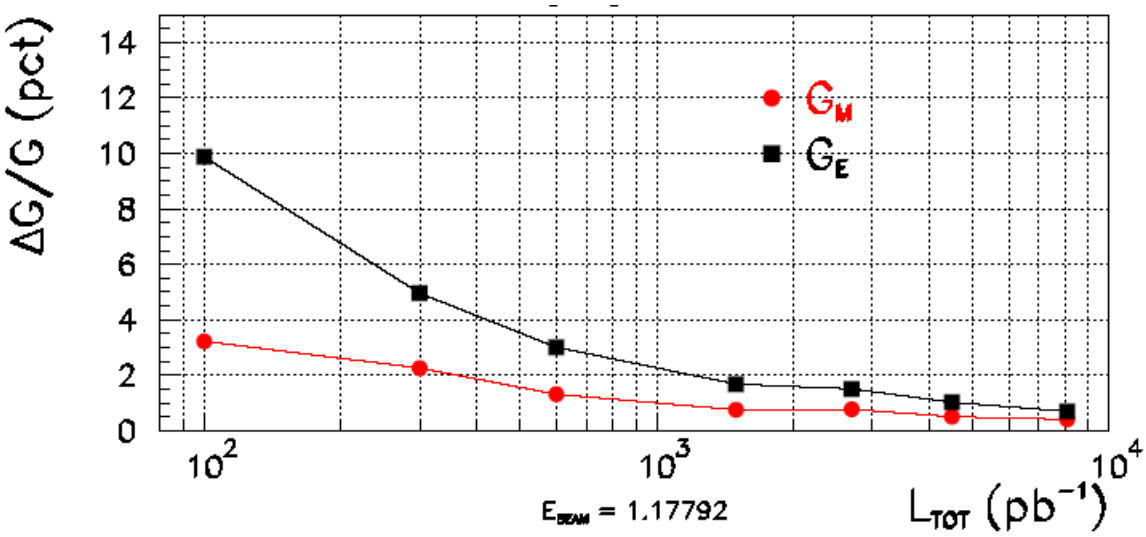

Fig. 18. *Relative error on the neutron FF as a function of the integrated luminosity for* E_{BEAM}*=1.2 GeV for the assumption* $|G_E^n| = |G_M^n|$.

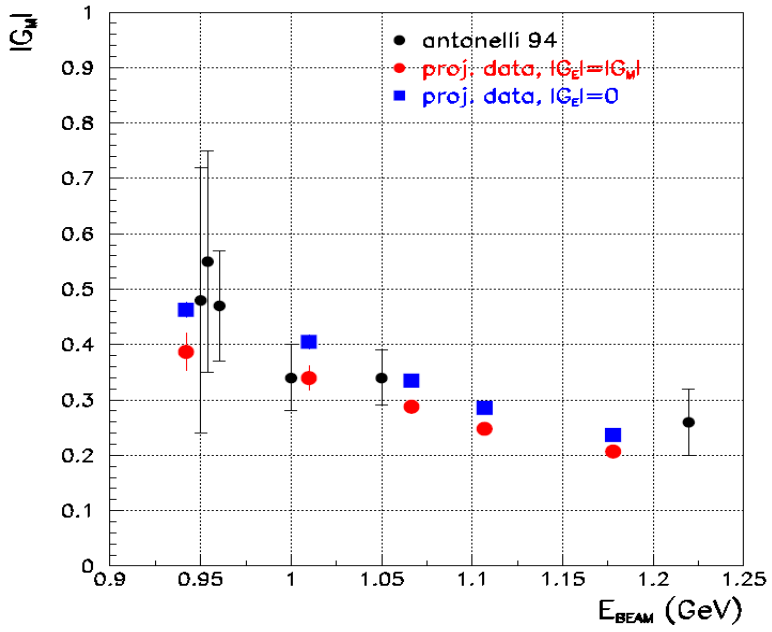

Fig. 19. *Projected neutron magnetic FF results for the two hypothesis on the electric to magnetic FFs ratio, compared with FENICE experimental data.*

measuring the left-rigth asymmetry with respect to the relevant axis

$$R = \frac{N_R - N_L}{N_R + N_L} = \frac{2}{\pi}\langle A_C \rangle \langle P_y \rangle, \tag{12}$$

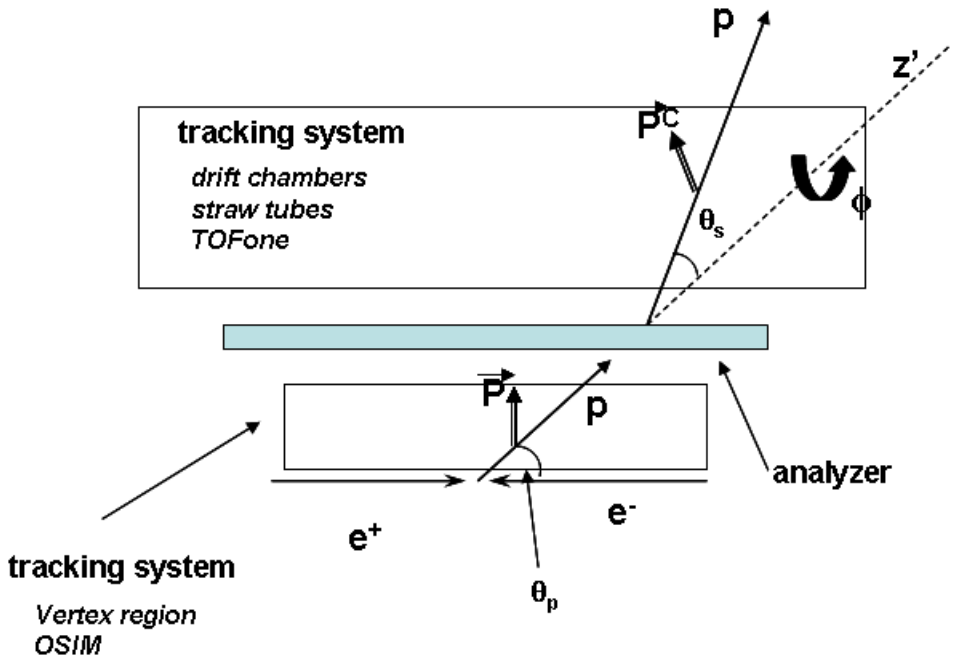

Fig. 20. *Sketch of the apparatus for the polarization measurement.*

$\sqrt{s}[MeV]$	$A_C[\%]$	$P_y[\%]$	R
2000	5.8	3.1	$1\ 10^{-3}$
2080	22	4.4	$6\ 10^{-3}$
2400	47	9.7	$3\ 10^{-2}$
3000	24	20	$3\ 10^{-2}$

Table 2
Average carbon analysing power and proton polarization (as taken from the curve in Fig. 8 and eq. (9)) in the energy range of interest.

where N_L (N_R) is the number of protons scattered on the left (right) with respect to the axis on the polarimeter plane. A rough counting rate estimate can be made using a reasonable polarimeter efficiency $\epsilon_{pol} \approx 3\%$. We then calculated:

- the average proton polarization $\langle P_y \rangle$ of eq. (12) in the FINUDA angular coverage (θ_p between 45^o and 135^o) from the values of the improved $(log^2 Q^2)/Q^2$ fit in Fig. 8 and from eq. (9);
- the analysing power $\langle A_C \rangle$ by averaging the experimental data [72] in the range of the secondary scattering angle θ_s between 5^o and 20^o.

The obtained values of $\langle A_C \rangle$ and $\langle P_y \rangle$, together with those of the ratio R, are reported in Tab. 2 for the beam energies of interest. As can be seen, under reasonable theoretical assumptions, one can estimate R to be of the order of

10^{-3} close to the threshold up to few percent for $E_{BEAM} \approx 1.2$ GeV. From these numbers, one can reasonably assume that the error on the measurement of the polarization will be largely dominated by the experimental statistical error on R:

$$\frac{\Delta R}{R} \approx \frac{1}{R\sqrt{N_R + N_L}}, \tag{13}$$

Given the values of R in Tab. 2 and the fast decrease of the total cross section (see Fig. 11), the most favourable beam energy should be around $E_{BEAM} = 1.2$ GeV, and an integrated luminosity of about 2500 pb^{-1} is necessary to have a 30% error on R (i.e. on P_y). This luminosity could be reached in approximately one year of data taking with an average luminosity of $10^{32} cm^{-2} s^{-1}$.
In principle, polarization measurement can be done together with the $p\bar{p}$ and $n\bar{n}$ cross section measurements, however, due to the low efficiency, probably a longer dedicated run will be necessary.

6 Λ-FORM FACTORS MEASUREMENTS WITH THE FINUDA DETECTOR

With a beam energy of at least about 1.2 GeV, it is possible to produce at DAΦNE-2 hyperons such as Λ or Σ, as shown in Fig. 11. Thus, it would be possible to measure hyperon FFs by studying the exclusive reaction $e^+e^- \to Y\bar{Y}$. They are related to the differential cross section and polarization observables by equations equal to that described for the nucleon, where the nucleon mass is replaced by the hyperon one. Apart from the DM2 cross section measurement [50] for $e^+e^- \to \Lambda\bar{\Lambda}$ at $s = 5.76$ GeV^2 (4 candidates only), there are no data on hyperon FFs. The cross section for $Y\bar{Y}$ should be few times smaller than the $N\bar{N}$ cross section (but DM2 found $\sigma(p\bar{p}) \approx \sigma(\Lambda\bar{\Lambda})$.

The $e^+e^- \to \Lambda\bar{\Lambda}$ reaction is particularly interesting, because the Λ polarization can be directly deduced by measuring its decay products, i.e. the proton and π^-. In fact, due to the weak nature of the decay, the nucleon is constrained to move preferentially in the direction of the hyperon spin, thus resulting in an asymmetric angular distribution with respect to the spin direction of the Λ. This asymmetry is the result of the interference between parity conserving (p-wave) and parity non conserving (s-wave) amplitudes. In the hyperon center-of-mass frame, the decay nucleon angular distribution is therefore of the form [73]

$$\frac{dN}{dcos\theta_p^{CM}} = N\left[1 + \alpha P_\Lambda cos\theta_p^{CM}\right], \tag{14}$$

where P_Λ is the magnitude of the Λ polarization, and θ_p^{CM} is the angle between the polarization axis and the proton momentum. The parameter α describes the interference between p- and s-wave in the weak decay, and has been measured to be $\alpha = 0.642 \pm 0.013$ [74].

As no polarimeter is required for Λ polarization measurements, higher efficiency is expected compared to the proton polarization measurements, presumably of the order of 50%.

Measurement of the exclusive $e^+e^- \to \Lambda\bar{\Lambda}$ reaction requires the full detection of the decay products of at least one of the two produced hyperons. The Λ lifetime is $c\tau = 7.89$ cm, thus the detection of detached vertex could help, but it's not necessary if the momentum resolution for protons and pions is good enough to clearly separate the $\Lambda\bar{\Lambda}$ events from the background of non resonant $e^+e^- \to p\bar{p}\pi^+\pi^-$ events. Fit of the angular distribution of the decay proton in the Λ rest frame with respect to the axis normal to the scattering plane will allow the extraction of P_Λ in eq. (14).

7 POSSIBLE IMPROVEMENTS OF THE FINUDA PERFORMANCE

The preliminary projection of the statistical accuracy described in Sects. 4 and 5 shows that the present FINUDA performance will allow the extraction of proton $|G_M^p|$ and $|G_E^p|$ with good precision. Assuming a cuncurrent running time, with the present neutron (or antineutron, with a suitable converter) detection efficiency, the FINUDA detector will allow the extraction of the neutron FFs with a relative error a few times bigger than for the proton (see Fig. 18). In the following, we will consider possible improvements in the detector to raise neutron precision to the same level as for the proton.

7.1 Neutron detection efficiency

One possibility is to use a second antineutron converter to double the detection efficiencies reported in Tab. 1. However, a second converter would also increase the minimum energy of the detected protons, thus one should make dedicated neutron runs.

Another possibility to increase the neutron detection efficiency could be the extension of the angular coverage of the TOFone barrel. This could be obtained by implementing a new array of scintillators, just before the end-cap (Fig. 12). As an example, by covering the angles from 20^o to 160^o one should reduce the

relative error by a factor of ≈ 2.

The increase of the neutron efficiency within the present angular coverage, for instance by increasing the thickness of the TOFone scintillators, seems not possible because of space limitations between the actual TOFone geometry and the magnetic coils. On the contrary, it could be possible to add a second layer of scintillators before the straw tubes. This could affect the overall resolution of the tracking system, and thus it must be carefully studied.

7.2 Neutron polarization

Neutron polarization can be measured through the scattering of the polarized neutron with unpolarized protons in the analyzer and by measuring the scattering angle of the emitted proton or neutron. The optimal choise for the analyzer could be a thin (few cm) plastic scintillator, as done in the NPOL3 polarimeter implemented at Los Alamos [75]. A typical efficiency of such a polarimeter is a few percent for neutron with kinetic energy of the order of 100 MeV. Thus, with the same integrated luminosity of 2500 pb^{-1} as for the proton, one should measure the neutron normal polarization with a statistical error a factor of ≈ 2 larger.

The FINUDA detector already includes the TOFino array of scintillator in the vertex tracking region, however its thickness of 0.2 cm seems to be too small to achieve sufficiently high efficiency. Thus, a new array of thicker scintillators could be implemented. It must be noted that, being rich of carbon, the scintillator could in principle be used to measure the proton polarization too.

8 TIME-LIKE NUCLEON FORM FACTOR MEASUREMENTS IN THE WORLD

The measurement of time-like proton FFs is part of the experimental program proposed for the HESR antiproton beam at GSI, which is expected to start in 2012. The PAX experiment [76] proposes to measure single and double spin asymmetry in the reversed channel $\bar{p}p \to e^+e^-$ [77], using polarized antiproton beams interacting with a transversely or longitudinally polarized proton target. Unpolarized measurements can be carried out independently at PAX as well as at PANDA [78] experiments. The use of single and double spin asymmetry will give access to several combination of $|G_M^p|$, $|G_E^p|$ and its relative phase δ_{ME}, allowing their extraction with small systematic uncertainties. For the proton FFs, these measurements would be the natural complement of

the measurement proposed in this letter. On the contrary, it must be stressed that neutron and hyperon FFs can only be accessed by using electron-positron collisions.

Measurements of the time-like nucleon FFs, in different and complementary energy regions, are also under consideration at Novosibirsk and Bejing.

9 SUMMARY

In view of the possible increase of the energy of the DAΦNE collider at Frascati above the nucleon-antinucleon threshold, we proposed a physics program to perform the full determination of nucleon and hyperon form factors.
A preliminary counting rate estimate with the FINUDA detector has been presented. This detector fulfills in an easy and satisfactory way all the main requirements of the proposed program.

Making a reasonable anticipation of the DAΦNE-2 performances, an integrated luminosity of the order of $100 pb^{-1}$ per beam energy (corresponding to few months of data taking) should allow the measurement of $|G_M|$ and $|G_E|$ at the few percent level for the proton and below 10% for the neutron.
Polarization measurements will allow the first determination of the relative phase between the electric and magnetic form factors. These measurements will require a longer dedicated run time or a better performance of the machine. The study indicates that the optimal beam energy for this measurement is close to $E_{BEAM} \approx 1.2$ GeV.

Measurements of hyperon-form factors will be also possible, provided the beam energy exceeds its energy threshold (s about 5 GeV). For the Λ-hyperon, the measurement of angular distribution of the decay proton in the Λ center-of-mass system gives the Λ-polarization, probably with much better statistical precision than for the proton.

The FINUDA detector is well suitable for the measurement, whithout major modifications. Nevertheless, possible improvements on the present layout have also been discussed. They include the extension of the TOFone scintilators array to improve the precision on the neutron form factor as well as the possible implementation of a neutron polarimeter.

References

[1] R.C. Walker *et al.*, Phys. Rev. **D49**, 5671 (1994).
C. Andivahis *et al.*, Phys Rev. **D50**, 5491 (1994).

[2] M.K. Jones *et al.*, Phys. Rev. Lett. **84**, 1398 (2000);
O. Gayou *et al.*, Phys. Rev. **C64**, 038292 (2001).

[3] O. Gayou *et al.*, Phys. Rev. Lett. **88**, 092301 (2002).

[4] V. Punjabi *et al.*, Phys. Rev. **C71**, 055202 (2005).

[5] E. Tomasi-Gustafsson, N. Cim. **C27**, 413 (2004).

[6] C.H. Hyde-Wright, K. de Jager, Annu. Rev. Part. Sci 2004, 54.

[7] H. Gao, Int. J. Mod. Phys. **E12**,1 (2003); Erratum-ibidem, **E12**,567 (2003).

[8] S.D.Drell and F.Zachariasen, Electromagnetic structure of the nucleons, Oxford University Press (1961).

[9] R. Baldini *et al.*, Eur. Phys. J. **C11**, 709 (1999); R. Baldini *et al.*, in *Proc. of the e^+e^- Physics at the intermediate Energies Conference*, edited by D. Bettoni, eConf **C010430**, T20 (2001) [arXiv hep-ph/0106006].

[10] B.V. Geshkenbein, B.L. Ioffe, M.A. Shifman, Yad. Fiz. **20**, 128 (1974).

[11] R. Calabrese, in *Proc. of the e^+e^- Physics at the intermediate Energies Conference*, edited by D. Bettoni, eConf **C010430**, W07 (2001); H.W. Hammer, *ibid.*, No. W08; C.E. Carlson, *ibid.*, No. W09; M. Karliner, *ibid.*, No. W10.

[12] R. Baldini *et al.*, Nucl. Phys. **A755**, 286c (2005).
R. Baldini *et al.*, hep-ph/0507085, submitted to Eur. Phys. J. C.

[13] For a recent review, see e.g:
K. Goeke, M.V. Polyakov, M. Vanderhaeghen, Prog. Part. Nucl. Phys. **47**, 401 (2001);
M. Diehl, Eur. Phys. J. **C25**, 223 (2003), Erratum-idid, **C31**, 277 (2003).

[14] A.V. Belitsky and A.V. Radyushkin, hep-ph/0504030.

[15] M. Guidal, M.V. Polyakov, A.V. Radyushkin and M. Vanderhaeghen, hep-ph/0410251.

[16] P.G. Blunden, W. Melnitchouk and J.A. Tjon, Phys. Rev. Lett. **91**, 142304 (2003) and nucl-th/0306076;
P.A.M. Guichon and M. Vanderhaeghen, Phys. Rev. Lett. **91**, 142303 (2003) and hep-ph/0306007;
M.P. Rekalo and E. Tomasi-Gustafsson, Nucl. Phys. **A740**, 271 (2004) and Eur Phys. J. **A22**, 331 (2004).

[17] A.V. Afanasev *et al.*, Phys. Rev. **D72**, 013008 (2005);
Y.C. Chen *et al.*, Phys. Rev. Lett. **93**, 122301 (2004).

[18] G. Blunden, W. Melnitchouk and J.A. Tjon, nucl-th/0506039.

[19] A. Afanasev *et al.*, JLab Experiment E-04-116.

[20] J. Arrington *et al.* nucl-ex/0408020.

[21] M.N. Rosenbluth, Phys. Rev. **79**, 615 (1950).

[22] C. Walker *et al.*, Phys. Rev. **D49**, 5671 (1994).
L. Andivahis *et al.*, Phys. Rev. **D50**, 5491 (1994).
J. Litt *et al.*, Phys. Lett. **B31**, 40 (1970).
C. Berger *et al.*, Phys. Lett. **B35**, 87 (1971).
L.E. Price *et al.*, Phys. Rev. **D4**, 45 (1971).
W. Bartel *et al.*, Nucl. Phys. **B58**, 429 (1973).

[23] A. Akhiezer and M.P. Rekalo, Dokl. Akad. Nauk USS, **180**, 1081 (1968) and Sov. J. Part. Nucl. **4**, 277 (1974);
G. Arnold, C.E. Carlson and F. Gross, Phys. Rev. **C23**, 363 (1981).

[24] B.D. Milbrath *et al.*, Phys. Rev. Lett. **80**, 452 (1998); Phys. Rev. Lett. **82**, 2221(E) (1999).

[25] J. Arrington, Phys. Rev. **C68**, 034325 (2003).

[26] I.A. Qattan *et al.*, Phys. Rev. Lett. **94**, 142301 (2005).

[27] E. Tomasi-Gustafasson and G. Garkh, hep-ph/04122137.

[28] C.F. Perdrisat, V. Punjabi, M.K. Jones, E. Brash *et al.*, Jefferson Lab. experiment P01-109.

[29] R.Madey and the Jefferson Laboratory E93-038 Collaboration, Phys. Rev. Lett. **91**,122002 (2003).

[30] S.J. Brodsky, G.R. Farrar, PhysṘev. **D11**, 1309 (1975); G.P. Lepage, S.J. Brodsky, Phys. Rev. **D22**, 2157 (1980).

[31] G.A. Miller and M.R. Franck, Phys. Rev. **C65**, 065205 (2002).

[32] A.V. Belitsky, X. Ji and F. Yuan, Phys. Rev. Lett. **91**, 092003 (2003).

[33] G. Hohler *et al.*, Nucl. Phys. **B114**, 505 (1976); M.F. Gari, W. Krumpelmann, Z. Phys. **A322**, 689 (1985); P. Mergell, U.G. Meissner, D. Drechsel, Nucl. Phys. **A596**, 367 (1996); E.L. Lomon, Phys. Rev. **C64**, 035204 (2001).

[34] F. Iachello, A.D. Jackson, A. Lande, Phys. Rev. Lett. **43B**, 191 (1973).

[35] Z. Dziembowski *et al.*, Ann. Phys. **258**, 1 (1997); S. Boffi *et al.*, Eur. Phys. J. **A14**, 17 (2002). G.A. Miller, Phys. Rev. **C66**, 032201 (2002).

[36] G. Holzwarth, Z. Phys. **A356**, 339 (1996).

[37] P.L. Chung, F. Coester, Phys. Rev. **D44**, 229 (1981); I.G. Aznaurian, Phys. Lett. **B316**, 391 (1993); F. Cardarelli *et al.*, Nucl. Phys. **A666-667**, 33c (2000).

[38] P. Kroll, M. Schurmann, W. Schweiger, Z. Phys. **A338**, 339 (1991); B.-Q. Ma, D. Qing, I. Schmidt, Phys. Rev. **C65**, 035205 (2002).

[39] D.H. Lu, A.W. Thomas, A.G. Williams, Phys. Rev. **C57**, 2628 (1998); D.H. Lu, S.N. Yang, A.W. Thomas, Report ADP 99-36/t373.

[40] A.V. Radyushkin, Acta Phys. Pol. **B15**, 40 (1984).

[41] S. Dubnicka, A.Z. Dubnickova ans P. Weisenpacher, J. Phys. **G29**, 405 (2003).

[42] F. Gross and P. Agbakpe, nucl-th/0411090.

[43] G. Cates, K. McCormick, B. Reitz, B. Wojtsekhowski, Jefferson Lab. xperiment E02-013.

[44] A.Z. Dubnickova, S. Dubnicka, P.M. Rekalo, N. Cim. **A109**, 241 (1996)

[45] C. Tzara, Nucl. Phys. **B18**, 246 (1970);

[46] A. Antonelli *et al.*, Phys. Lett. **B365**, 427 (1996).

[47] A. Antonelli *et al.*, Phys. Lett. **B313**, 283 (1993); A. Antonelli *et al.*, Nucl. Phys. **B517**, 3 (1998).

[48] B. Delcour et *al.*, Phys. Lett. **B86**, 395 (1979).

[49] D. Bisello et *al.*, Nucl. Phys. **B224**, 379 (1983).

[50] D. Bisello et *al.*, Z. Phys. **C48**, 23 (1990).

[51] G. Stancari, PhD Thesis, Ferrara University (1998);
M. Andreotti, Laurea Thesis, Ferrara University (2001).

[52] M. Castellano *et al.*, Il N. Cim. **14A, 1** (1973).

[53] A. Antonelli *et al.*, Nucl. Phys. **B517**, 3 (1998).

[54] G. Bassompierre *et al.*, Phys. Lett. **B68**, 477 (1977).

[55] G. Bardin *et al.*, Nucl. Phys. **B411**, 3 (1994).

[56] T.A. Armstrong *et al.*, Phys. Rev. Lett. **70**, 1212 (1992).

[57] M. Ambrogiani *et al.*, Phys. Rev. **D60**, 032002 (1999).

[58] M. Andreotti *et al.*, Phys. Lett. **B559**, 20 (2003).

[59] R. Baldini, E.P.S. Conference, Lisbon, July 21-27, 2005.

[60] A.A. Logunov, N. van Hieu, I.T. Todorov, Ann. of Physics, **31**, 203 (1965).

[61] S.M. Bilenky, C. Giunti, V. Wataghin, Z. Phys. **C59**, 475 (1993).

[62] N. Cabibbo, R. Gatto, Phys. Rev. **124**, 1577 (1961);
R. Felst, DESY Internal Note 73/56 (1973);
J.G. Korner, M. Kuroda, Phys. Rev. **D16**, 2165 (1977);
P. Cesselli, M. Nigro, C. Voci, Proc. of Workshop on Physics at LEAR, Erice (1982);
E. Etim, A. Malecki, LNF Internal Note LNF-89-023 (1989);
S. Dubnicka, N. Cim. **A100**, 1 (1988); **A103**, 469 and 1417 (1990); **A104**, 1075 (1991);
S.I Bilenkaya, S. Dubnicka, A.Z. Dubnickova, P. Strizenec, N. Cim. **A105**, (1992).

[63] J. Ellis, M. Karliner, H. Kowalski, P. Lett. **B235**, 341 (1990).

[64] S. Rock, *Proc. of the e^+e^- Physics at the intermediate Energies Conference*, edited by D. Bettoni, eConf **C010430**, W14 (2001) [arXiv hep-ph/0108106].

[65] S.J. Brodsky, C.E. Carlson, J.R. Hiller and D.S. Hwang, Phys. Rev. **D69**, 054022 (2004); H.W. Hammer, U.G. Meissner, arXiv hep-ph/0312081.

[66] M. Gari, W. Krmpelmann, Z. Phys. **A322**, 689 (1985). E.L. Lomon, Phys. Rev. **C66**, 045501 (2002); **64**, 035204 (2001).

[67] C.C. Kuo *et al.*, hep-ex/0503006;
M. Artuso *et al.*, Phys. Rev. **D50**, 5484 (1994);
H. Hasamaki *et al.*, Phys. Lett. **B407**, 185 (1997);
G. Abbiendi *et al.*, Eur. Phys. J. **C28**, 45 (2003);
P. Achard *et al.*, Phys. Lett. **B571**, 11 (2003).

[68] D. Alesini *et al.*, Frascati Note G-63.

[69] The KLOE Collaboration - KLOE: A general purpose detector for DAΦNE - LNF-92/019(IR).

[70] FINUDA Collaboration, *Finuda, a detector for Nuclear Physics at DAΦNE*, LNF Preprint LNF-93/021(IR), 1993.

[71] A. Filippi, Proc. of *Workshop on e^+e^- in the 1-2 GeV range: Physics and Accelerator Prospects*, 10-13 September 2003, Alghero, Italy.

[72] T. Pospischil *et al.*, NIM **A483**, 713 (2002).

[73] B.E. Bonner *et al.*, Phys. Rev. **D38**, 729 (1988).

[74] C. Caso *et al.*, Rev. of Particle Physics, Eur. Phys. J. **C3**, 1 (1998).

[75] T. Wakasa *et al.*, nucl-ex/0502006.

[76] PAX Collaboration, *Antiproton-Proton Scattering Experiments with Polarization*, Letter of Intent, hep-ex/0505054.

[77] E. Tomasi-Gustafsson *et al*, Eur. Phys. J. **A24**, 419 (2005).

[78] PANDA Collaboration, *Antiproton Physics at Darmstadt*, Letter of Intent GSI-ESAC/Pbar, 21 Jan. 2004.